Biological and Medical Applications of Materials and Interfaces

Dual role of magnetic nanoparticles as intracellular hotspots and extracellular matrix disruptors triggered by magnetic hyperthermia in 3D cell culture models

Lilianne L. Beola, Laura Asín, Raluca Maria M Fratila, Vanessa Herrero, Jesús M. De La Fuente, Valeria Grazu, and Lucía Gutiérrez

ACS Appl. Mater. Interfaces, **Just Accepted Manuscript** • DOI: 10.1021/acsami.8b18270 • Publication Date (Web): 27 Nov 2018

Dual Role of Magnetic Nanoparticles as Intracellular Hotspots and Extracellular Matrix Disruptors Triggered by Magnetic Hyperthermia in 3D Cell Culture Models

Lilianne Beola[†,#], Laura Asín,[†,‡, #,] Raluca M. Fratila[†,‡], Vanessa Herrero[†], Jesús M. de la Fuente[†,‡], Valeria Grazú[†,‡] and Lucía Gutiérrez[†,‡,§*,]*

[†]*Instituto de Ciencia de Materiales de Aragón (ICMA), CSIC/Universidad de Zaragoza, C/ Pedro Cerbuna 12, 50009, Zaragoza, Spain.*

[‡]*Centro de Investigación Biomédica en Red de Bioingeniería, Biomateriales y Nanomedicina (CIBER-BBN), 50018, Spain.*

[§] *Department of Analytical Chemistry, Instituto Universitario de Nanociencia de Aragón (INA), Universidad de Zaragoza, Edificio I+D, Mariano Esquillor Gómez, 50018, Zaragoza, Spain*

 # Shared first author

**L.A.: lasin@unizar.es; L.G.: lu@unizar.es*

Keywords: iron oxides, magnetic nanoparticles, hyperthermia, 3D cell culture, macrophages, cell death, collagen.

Abstract

Magnetic hyperthermia is a promising therapy for the localized treatment of cancer based on the exposure of magnetic nanoparticles to an external alternating magnetic field. In order to evaluate some of the mechanisms involved in the cellular damage caused by this treatment, two different 3D cell culture models were prepared using collagen, which is the most abundant protein of the extracellular matrix. The same amount of nanoparticles was added to cells either before or after their incorporation to the 3D structure. Therefore, in one model, particles were located only inside cells (*In model*), while the other one had particles both inside and outside cells (*In&Out model*).

In the *In&Out model*, the hyperthermia treatment facilitated the migration of the particles from the outer areas of the 3D structure to the inner parts, achieving a faster homogeneous distribution throughout the whole structure and allowing the particles to gain access to the inner cells.

The cell death mechanism activated by the magnetic hyperthermia treatment was different in both models. Necrosis was observed in the *In model* while apoptosis in the *In&Out model* 24 hours after the hyperthermia application. This was clearly correlated with the amount of nanoparticles located inside the cells. Thus, the combination of both 3D models allowed us to

demonstrate two different roles of the magnetic particles during the hyperthermia treatment: i) *The modulation of the cell death mechanism depending on the amount of intracellular particles,* and ii) *The disruption of the collagen matrix caused by the extracellular nanoparticles.*

Introduction

Iron oxide magnetic nanoparticles (MNPs) are one of the most promising systems within the field of biomedicine and biotechnology.[1-3] Their physico-chemical characteristics as well as their magnetic properties, provide unique opportunities for the development of a wide range of applications such as biosensors,[4-5] controlled drug delivery systems,[6-7] contrast agents for magnetic resonance imaging,[8-9] or cancer therapies such as magnetic hyperthermia.[10]

Magnetic hyperthermia (MH) has been particularly studied in recent years for the treatment of malignant tumours.[11-13] It is widely known that cancer cells are more sensitive to heat than normal cells.[14] MNPs act as localized heating sources in the region where they are situated when submitted to an alternating magnetic field (AMF).[15] The local temperature increase in the tumour area induces cell death or alters the growth and differentiation of the cancer cells.[16] At the same time, MH has been used to promote synergistic effects when combined with other conventional treatments. In particular, it has been shown that MH treatment makes the cells more sensitive to radiation or to the action of certain chemotherapeutic drugs.[17-19] A possible explanation of this synergistic effect between heat and chemotherapy was given by Krawczyk *et al.* who demonstrated that mild hyperthermia conditions provoked the degradation of BRCA2, a protein involved in the homologous recombination, which is a DNA repair mechanism by which the double strands breaks are repaired. If the cells are deficient in this DNA repair mechanism they become more sensitive to drugs that induce DNA damage.[20]

The cell death mechanisms activated by the MH treatment and the relevant parameters that control the triggering of each mechanism are not completely known yet. The classical conception of two cell death routes, apoptosis and necrosis, which take place independently, has been already refuted. Besides, some classical postulates about these two cell death mechanisms have been progressively abandoned and replaced for new ideas. It is known that necrosis can take place in a regulated way, like apoptosis, and that the apoptotic cells can sometimes be recognized by the immune system and trigger an adaptive immune response, like necrosis. Nevertheless, it is crucial to be able to control the activation of either necrosis

or apoptosis mechanisms and to try to control the pro-inflammatory immune response that could be sometimes negative for tumour treatments, as it involves non-desirable processes such as the tumour invasion or metastasis. [21-23]

Currently, most of the *in vitro* studies that analyse the efficacy of the hyperthermia treatment are being performed in monolayer cell cultures.[24-26] However, this traditional cell culture method, in two dimensions (2D), has essential limitations in terms of inter-cellular communication, cell microenvironment and cell spatial behaviour.[27] Therefore, these 2D cell culture models cannot replicate the morphology and biochemical properties the cells have in the living organisms. They also lack the complex scenario that the MNPs face to reach the deeper areas of the tumours. One of the alternatives to solve these problems is the use of three dimensions (3D) cell culture models, such as spheroids, liquid spheres,[28-29] or 3D scaffolds.[30-31] 3D cell culture models are simple structures that mimic more accurately the tumour composition and structure[32] providing a more realistic environment to evaluate the cellular response to a treatment [33]. In addition, 3D cell culture models allow the production of a high number of identical replicas and provide a good alternative to perform preliminary tests before *in vivo* experimentation allowing the reduction of the number of animals needed. Until know, the number of studies using 3D cell culture models to evaluate the effect of magnetic hyperthermia is still scarce.[34] These previous studies have mainly used spheroids as 3D cell cultures, a model that lacks the presence of extracellular matrix.

In this work, we have developed two 3D cell culture models based on the use of a collagen matrix to evaluate the efficacy of magnetic hyperthermia treatment in a murine macrophage/monocyte cell line (RAW 264.7). Collagen was selected because besides being one of the major components of the extracellular matrix (ECM), it also plays a crucial role in the tumour ECM.[35] In particular, tumours with well-organized and highly interconnected collagen fibres display lower penetration of high-molecular-weight chemotherapeutic agents than those with disordered and loose collagen networks.[36 37] Macrophages were chosen as model cells due to their known capacity of easily incorporating iron oxide nanoparticles.[38] This fact allowed working with a wide range of concentrations of nanoparticles inside the cells, which facilitated the study of the correlation between the amount of internalized particles and the cell death mechanism activated. The main difference between the two models is the moment in which MNPs are in contact with the cells along the 3D cell culture preparation protocol. In one model (*In Model*), cells in suspension are incubated with the particles and after washing away the MNPs that have not been internalized, the cells are transferred to form the 3D matrix, thus resulting in a homogeneous internalization of the

MNPs amongst all the cells and also an exclusive intracellular location of the MNPs. The other model is based on the administration of the MNPs to the cells once they are already forming part of the 3D matrix resulting in a model where particles need time to penetrate and fill up the whole 3D matrix to gain access to inner cells. As a result, this model allows obtaining a different MNP distribution than the former approach, having particles located both inside and outside the cells (*In&Out Model*) (Fig. 1). The combination of both models allows disentangling the effect that MNPs have on the extracellular matrix and the treatment efficiency.

In this work, we have used confocal microscopy and flow cytometry to study the MNP uptake, with and without exposure to an AMF. We have studied the evolution of the MNP location within the collagen matrix after the AMF exposure. We have also evaluated the cell death mechanisms triggered by the treatment at different times post-treatment (0, 24 and 48 h). Cell cycle and the cell viability studies allowed to discriminate the cell death mechanisms observed 24 h after MH treatment which was different on each 3D model: necrosis for the *In Mode* and apoptosis in the case of the *In&Out Model*. Besides, we have analysed the amount of MNPs internalized in each 3D model in order to establish a relationship between their concentration and the cell death mechanism observed after the treatment.

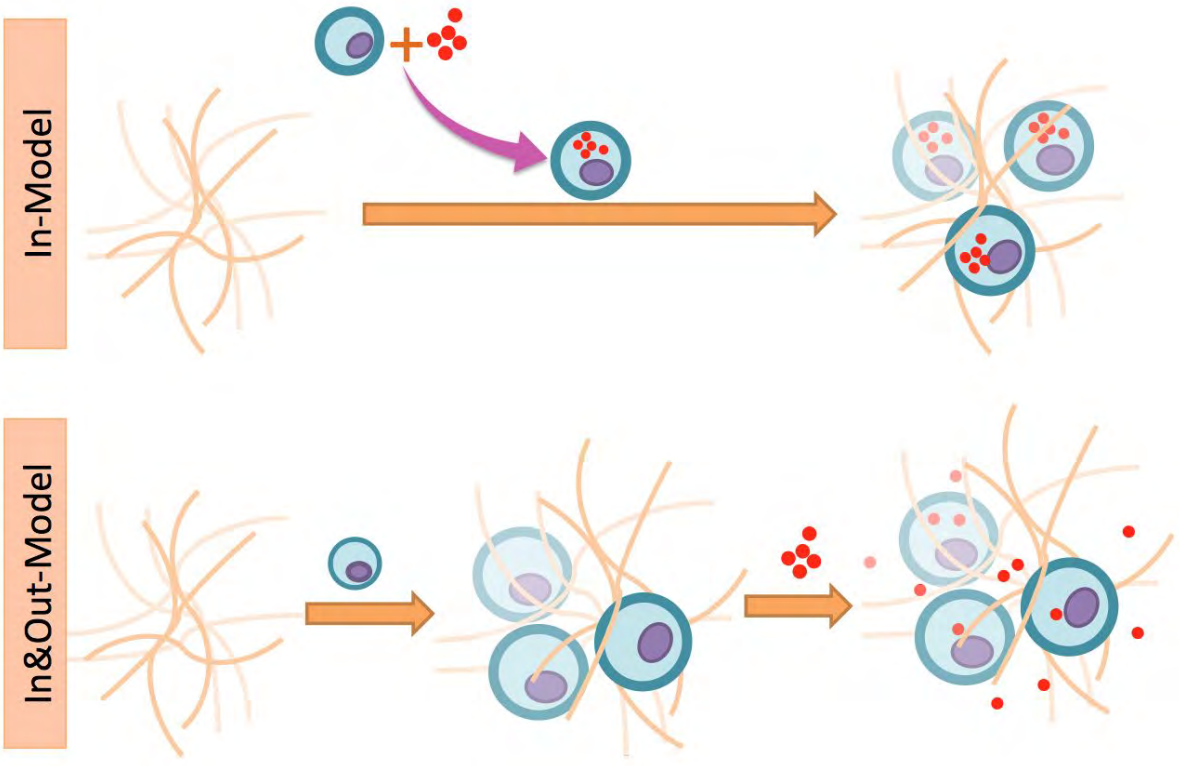

Fig. 1. ***Representation of the formation of the two 3D models used in this work.*** *In Model, where the MNPs are located just inside the cells. In&Out Model, where MNPs are located both inside and outside the cells.*

Results and discussion

We have chosen spherical 11 nm iron oxide MNPs (11.2 ± 0.8 nm, Fig. 2), as this diameter is within the most commonly studied range for *in vivo* magnetic hyperthermia experiments.[39] This diameter fulfils the requirements for *in vivo* experimentation, as it avoids fast renal clearance. This size is also considered to be in the range to achieve the better heating properties for magnetite/maghemite.[40]

MNPs have been prepared by thermal decomposition to have a careful control of the particle size and size distribution (Fig. 2). The superparamagnetic behaviour at room temperature, desired in many biomedical applications to prevent the MNP aggregation associated to a permanent magnetic moment,[1] has been verified by magnetic measurements confirming the negligible coercivity and also indicating the good crystalline properties of the prepared material by a high saturation magnetization (M_s = 81 Am^2/kg Fe_3O_4) (Fig. 1).

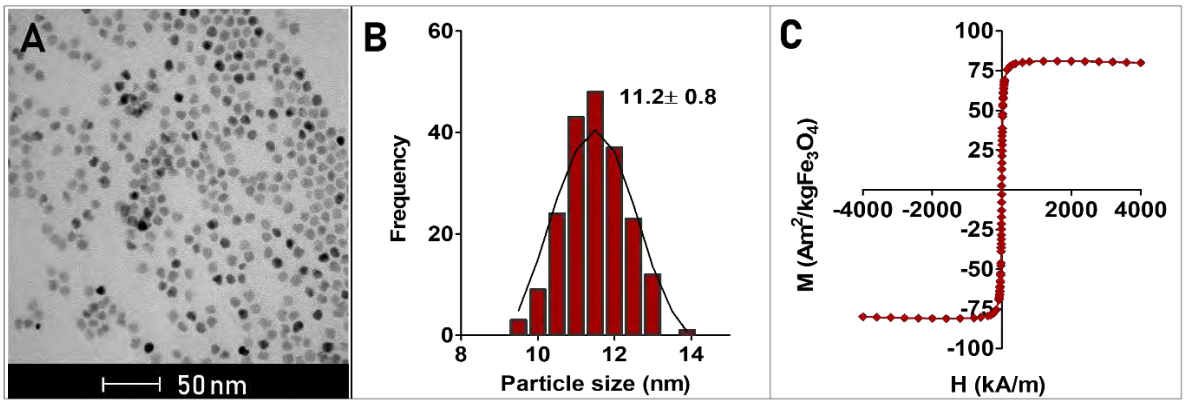

Fig. 2. ***Magnetic nanoparticle characterization.*** *(A) TEM micrograph, (B) Particle size distribution analysis and (C) Field dependent magnetization of the MNPs in water.*

MNPs have been subsequently coated with a polymer (PMAO, poly (maleic anhydride-alt-1-octadecene) modified with a fluorophore (TAMRA, Carboxytetramethylrhodamine). The polymer coating allows the transference of the magnetic cores from the organic to the aqueous phase and provides carboxylic groups that allow both the incorporation of the fluorophore, to track the location of the MNPs in the *in vitro* experiments, and glucose, to prevent the aggregation in cell culture medium and provide an active targeting molecule for the particles uptake.[41] Glucose is especially interesting in our case as macrophages, as well as

many tumour cells, due to their high energy requirements present upregulated glucose transporter proteins and subsequently the uptake of glucose-functionalized MNPs is enhanced.[42] The successful glucose functionalization, routinely used in our lab, [43] has been verified by ζ – potential measurements through a significant decrease of the MNP negative charge from -36 mV, before functionalization, to -13 mV after the glucose addition.

Several tests have been performed to assure that the material was suitable for *in vitro* experiments. Stability of functionalized MNPs has been assessed by Dynamic Light Scattering (DLS) measurements, showing that the hydrodynamic size of the particles before and after the glucose functionalization remains below 70 nm for MNPs at pH = 7, suspended both in water and complete culture medium (with 10% Foetal Bovine Serum) (Table. S1, Supporting Information). In addition, a sterility assay was performed and no evidence of the presence of microbial colonies has been observed after performing the test with the MNPs (Fig. S1, Supporting Information). Finally, although the low toxicity of particles prepared following the same protocol has already been checked in the past,[44-45] cell viability after the MNP administration was studied by flow cytometry in 2D cell culture models at different concentrations up to 100 μg of Fe per well (200 μg/ml), observing only a significant reduction of the cell viability at the highest concentration (Fig. S2, Supporting Information). From these results, an iron amount of 100 μg of Fe per well has been chosen for the hyperthermia experiments, as it is the highest concentration tested in which the viability is not significantly different to the controls. The low toxicity of this amount of MNPs has also been confirmed by flow cytometry in the 3D cell cultures (Fig. S3, Supporting Information).

The heating efficiency of the MNPs in water suspensions has been evaluated before the *in vitro* test. The Specific Absorption Rate (SAR) of the MNPs measured at an iron concentration of 1 mg/mL and using a field amplitude of H = 20 kA/m, and a frequency of 829 kHz is 253 W/g Fe. Establishing a correlation between the heating capacity of the MNPs in suspension and their ability to heat efficiently in *in vitro* experiments is not straightforward. First, it is difficult to determine and mimic the aggregation degree of the MNPs in the cellular environment. It is also a complex task to know the local concentration of the MNPs once they have been internalized by the cells. However, until all these problems are solved, the most common approach to validate that a specific material produces heat in the presence of an AMF is to measure the change of temperature over time in water at physiological pH, as at least it provides some information for comparison with other reported values.

Two different 3D cell culture models have been developed. To achieve the generation of two 3D cell culture models we have followed two different strategies for the incubation of the cells with magnetic nanoparticles. As a proof of concept, macrophages have been selected as a model cell line, as they are known to easily uptake this kind of particles.[38, 46]

The first approach followed has been to incubate the detached macrophages with the MNPs and, after removal of the particles that were not internalized, to form the 3D cell culture with the cells containing the MNPs. This approach leads to a 3D cell culture in which the MNPs are homogeneously distributed amongst all the cells and only located inside them (*In Model*), as observed by confocal microscopy and flow cytometry (Fig. 3), showing that almost all the cells (> 99%) contained MNPs after 1 h of incubation time.

The second approach has been to embed the macrophages within the 3D structure and then administer the MNPs. This way, particles need more time to penetrate the collagen structure to reach the inner cells. Although, after the incubation time, the supernatant is removed and the 3D structure is washed, some MNPs remain within the collagen matrix outside the cells. Because in this model particles could be found located both inside and outside the cells, we have named it "*In&Out Model*". The presence of particles both inside the cells and within the collagen matrix has been verified by confocal microscopy (Fig. 3). Interestingly, two different cell populations have been identified by flow cytometry: one population of cells with particles (58 ± 5%) and the other without particles (42 ± 8 %), indicating a slower rate of MNP uptake when compared to the *In Model* for the same incubation time of 1 h (Fig. 3), probably due to the time required for the movement of the MNPs towards the inner parts of the 3D structure. One of the advantages of using these two 3D cell culture models is that, although the same amount of particles has been administered to the cells, we have been able to achieve two different kinetic behaviours of MNP internalization.

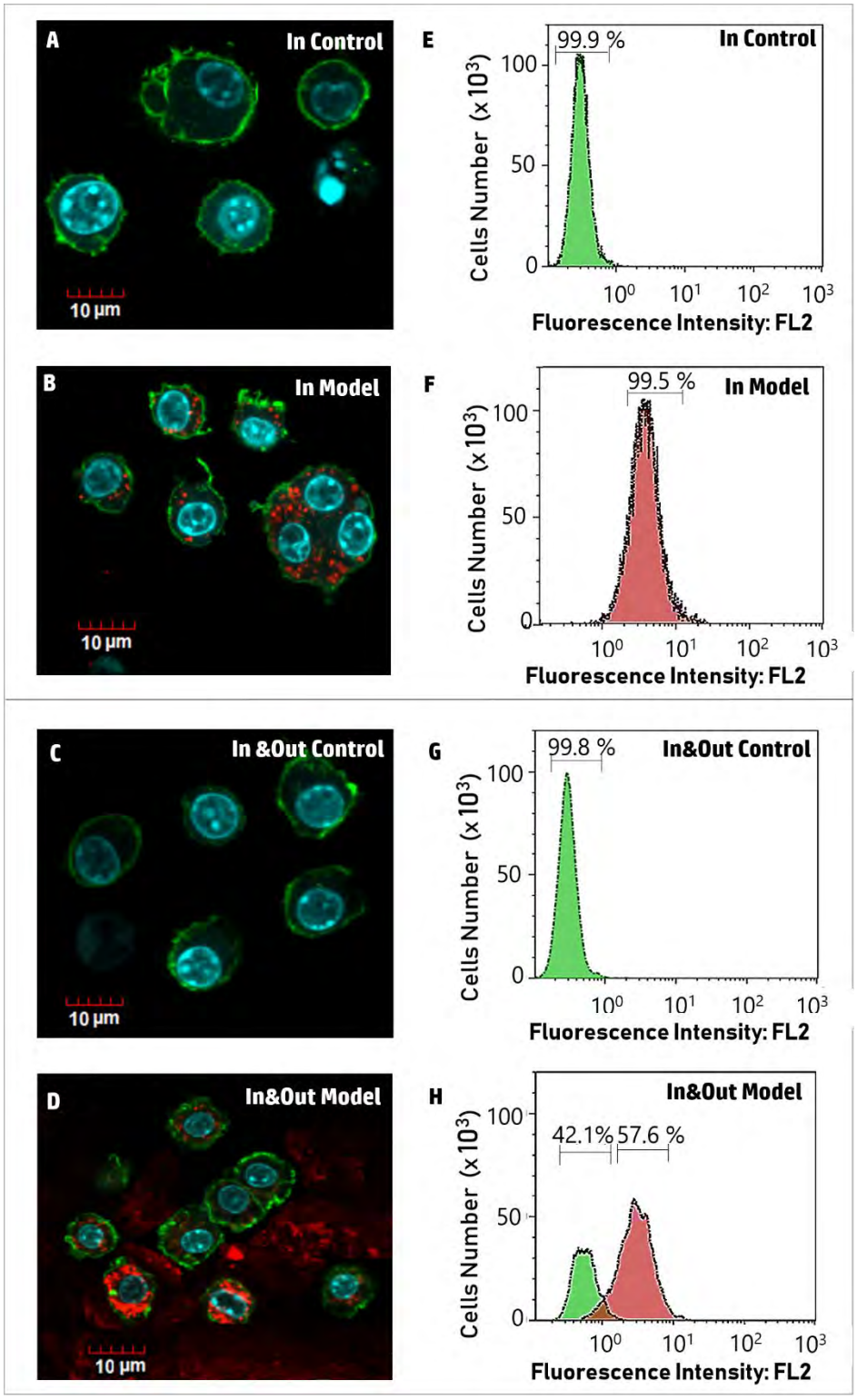

Fig. 3. ***3D cell culture characterization*** *(A, B, C, D) Confocal images. The nucleus is shown in blue (DAPI), actin in green (Phalloidin_AlexaFluor488) and MNPs in red (TAMRA). Scale bar: 10 µm. (E, F, G, H) Flow cytometry analysis of nanoparticle uptake. Data have been selected as a representation of a series of five experiments.*

AMF exposure enhances MNP uptake. Once it has been verified that the two models were successfully generated, the transformations that may occur with time have been evaluated. In particular, the capacity of the cells to continue internalizing MNPs in the *In&Out Model* has been assessed. To evaluate the time frame of the MNP uptake in the *In&Out Model*, the evolution with time of the two different cell populations previously observed by flow cytometry (with and without MNPs) has been measured (Table 1). Results have been compared also with 3D cell cultures of the *In&Out Model* after the AMF exposure to evaluate its impact on the MNP uptake.

The percentage of cells that contain MNPs in the *In&Out Model* increases with time, reaching a point at 24h after their addition where all cells contain MNPs (Fig. 4). This uptake, however, is significantly faster in the 3D cell cultures exposed to the AMF. It has been observed that immediately after the AMF exposure, a higher percentage of cells had uptaken MNPs (70 ± 3 %) in comparison with the control experiment with no AMF exposure in which only 58 ± 4 % of the cells showed MNP internalization. In addition, 3 h after the administration of the MNPs, the two populations of cells (with (69 ± 4 %) and without (31 ± 4 %) particles) were still observed in the 3D cell culture that had no exposure to the AMF while almost all the cells exposed to the AMF (99 ± 0.5 %) had uptaken MNPs. Nevertheless, although all the cells from the *In&Out Model* contain MNPs 24 h after the 3D cell culture generation, still many particles remain located outside the cells within the collagen fibres as observed by confocal microscopy (Fig. 5). As a conclusion of these results, flow cytometry studies in the *In&Out Model* demonstrate an enhancement in the rate of the MNP uptake by the cells triggered by AMF exposure (Fig. 4).

Experimental conditions	**Time points**		
	0 h	**3 h**	**24 h**
-AMF	58 ± 4 %	69 ± 4 %	99.5 ± 0.3 %
+AMF	70 ± 3 %	99 ± 0.5 %	99.2 ± 0.6 %

Table 1. ***Percentage of cells that contain MNPs in the In&Out Model at different time points, either in the control experiment with no AMF exposure (-AMF) or after the AMF exposure (+AMF).*** *Data obtained by flow cytometry (n=5).*

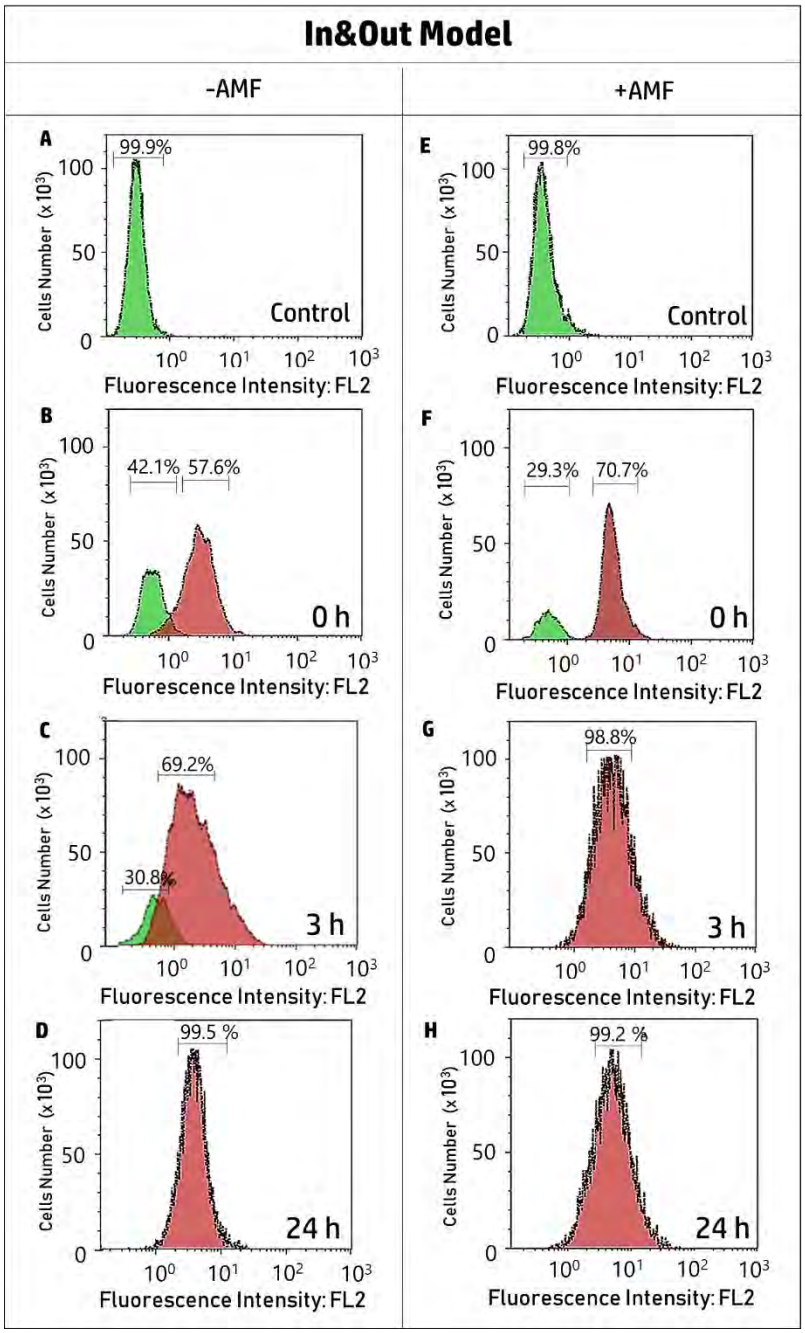

Fig. 4. ***Flow cytometry analysis of the time dependent nanoparticles uptake in the In&Out Model.*** *Left: Cells without exposure to the AMF (-AMF), Right: Cells after the AMF exposure(+AMF). (A, E) Control cells without MNP, (B, F) 0 hours, (C, G) 3 hours, (D, H) 24 hours. Data have been selected as a representation of a series of five experiments.*

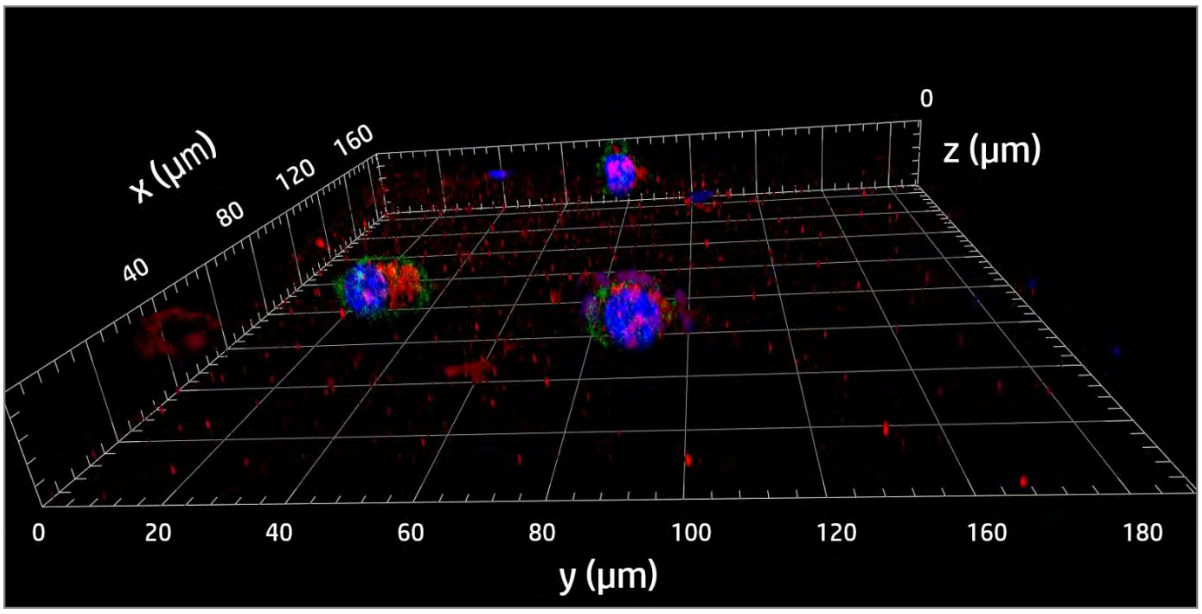

Fig. 5. ***3D reconstruction of confocal images acquired for the In&Out Model 24 h after AMF exposure****. The nucleus is shown in blue (DAPI), actin in green (Phalloidin_AlexaFluor488) and MNPs in red (TAMRA). The presence of MNPs is still observed outside the cells 24 h after the AMF exposure.*

To further investigate the mechanisms behind this MNP internalization enhancement mediated by AMF exposure, two 3D cell cultures of the *In&Out Model* have been prepared, and one of them has been exposed to the AMF. Images of the whole 3D structure have been acquired for the initial time point (Fig. 6). In the case of the cell culture not exposed to the AMF, most of the particles have not been able to diffuse towards the inner part of the collagen matrix, being mainly localized in the outer areas of the 3D structure. However, in the cell culture exposed to the AMF, particles have penetrated better and are more homogeneously distributed throughout the whole 3D structure. This phenomenon of a more uniform distribution of MNPs after the AMF exposure has also been previously observed in a spheroid model of triple negative breast cancer.[34] It has also been previously reported on a *in vivo* model where the nanoparticles where initially located in the collagen-rich outer areas of the tumour and penetrated more deeply into the core after the hyperthermia treatment.[47]

The enhancement of the MNP uptake may be associated with an increase in collagen permeability induced by the temperature rise during the MH treatment making the MNPs more “accessible” to the cells. It is known since a long time that the melting temperature of the triple helixes of the collagen type I, which is the most abundant in the nature, is few

degrees above body temperature.[48] Most recent studies have shown that the denaturation of the collagen vitrified gels takes place in two steps: a reversible process that results in a meta-stable collagen matrix, and an irreversible process that takes place at 60 ºC, leading a random uncoiled collagen.[49] These results are relevant for the design of future preclinical treatments, as collagen is one of the major components of the tumour extracellular matrix present in breast,[50] prostate,[51] glioma,[52] or pancreatic[53] cancer. Therefore, the benefits of the application of periodical cycles of AMF exposure would be to improve the permeability of the extracellular matrix and therefore the access of chemotherapeutic drugs or cells from the immune system to the inner areas of the tumour. In addition, the enhancement of the internalization of MNPs after each cycle could positively influence subsequent hyperthermia cycles and this amplification effect could have positive synergetic effects in the final effectiveness of the treatment.

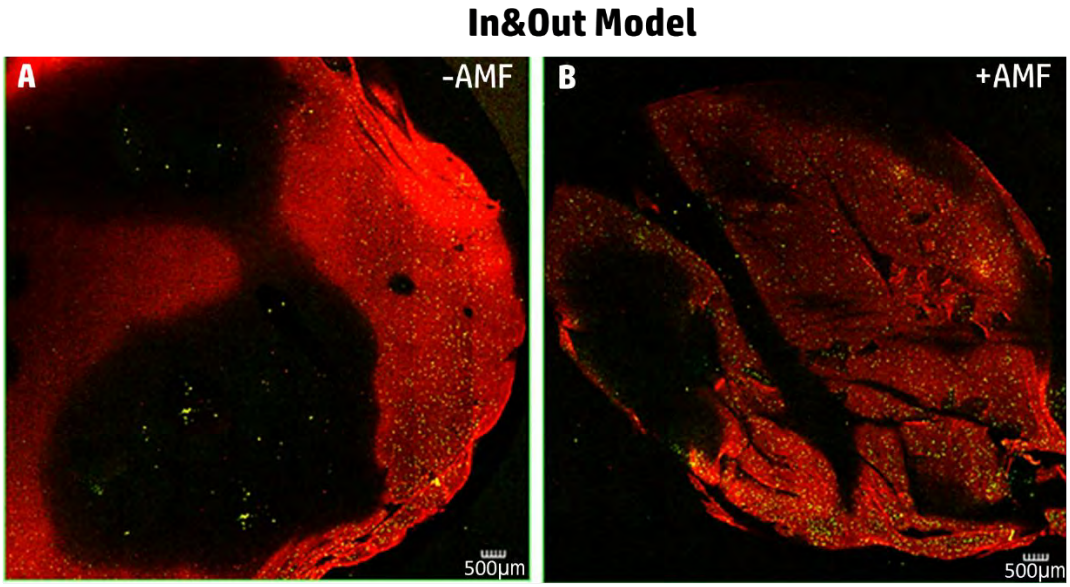

Fig. 6. ***Map image of confocal microscopy of 3D cell culture without (A) and with (B) the AMF exposure for the In&Out Model (0 hours).*** *The image shows the overlay of two channels: green fluorescence of the labeled cells and red fluorescence of the MNPs. Scale bar is 500 µm.*

Magnetic Hyperthermia treatment induces different cell death mechanisms in the two 3D cell culture models. To evaluate the effect of the differences between the two models on the cell death mechanisms we have evaluated the activation of the cell death routes at three different time points (0, 24 and 48 h) after the hyperthermia treatment. Interestingly, the results have shown differences in the cell death mechanism between the two models. Just

after the hyperthermia treatment (0 h) most of the cells remain alive in both models, being negative for Propidium Iodide (PI) and Annexin V staining. PI is a small molecule that enters in the cells and binds DNA only when the lipid bilayer membrane is disrupted, which happens in the late stages of the apoptosis and in the necrosis mechanism. Annexin-V binds phosphatidylserine (PS), a phospholipid that is normally located on the inner side of the cell membrane but translocates to the extracellular side in the first stage of the apoptosis. Therefore, cells that are positive for PI and negative for Annexin V have their cell membrane integrity altered without exposing the phosphatidylserine, a process typical from the beginning of necrosis, while cells that are positive for both markers indicate a late necrosis or late apoptosis stage.[54]

One day after the treatment, the *In Model* shows a significant population of necrotic cells (39.02 ± 4%) (positive for PI and negative for Annexin V), 60.09 ± 4.5% of cells that are still alive (negative for both markers) and a small percentage of cells (0.89 ± 0.1%) that are probably in a late necrosis stage (positive for both markers). On the contrary, at 24 h, the *In&Out Model* presents a very different situation where 38 ± 5.6% of the cells are undergoing apoptosis (positive for Annexin V and negative for PI) and the rest of the cells (61 ± 5.8%) are alive (Fig. 7). As a conclusion we can say that the *In&Out Model* results in a more controlled cell death pathway while the response to the MH treatment in the *In Model* is more aggressive.

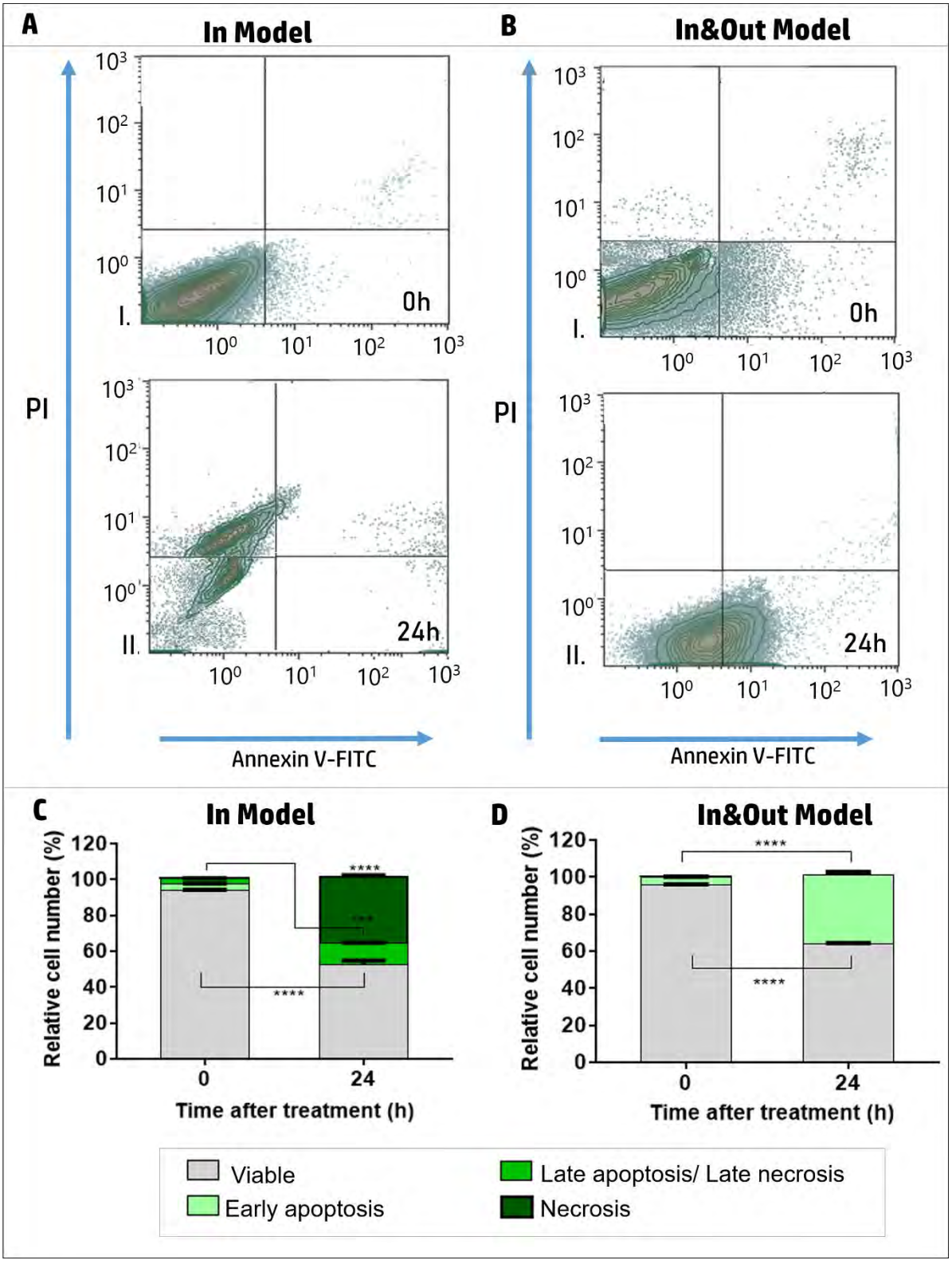

Fig. 7. ***Analysis of magnetic hyperthermia-induced cell death (Annexin V and PI staining).*** *Selected density plot (representative of 5 experiments) obtained at 0h and 24h after MH treatment for the In Model (A) and In&Out Model (B). (C and D) Summarized flow cytometry data resulting from five independent experiments shown as mean ± SD. Statistical significance between the means at the different times was determined using a two-way*

*ANOVA with Sidak's multiple comparisons test (**** $p < 0.0001$; *** $p < 0.001$; $p > 0.05$ no significance).*

To evaluate the status of the cells that remain alive 24 h after the treatment, the cell cycle has been analysed by flow cytometry (Fig. 8). It has been previously shown that among the crucial events triggered by a heat shock stress are the changes in the cell cycle progression. Depending on the duration and the intensity of the heat shock, cells can enter into a transient or permanent cycle arrest that can take place either in the G1 or G2/M transition. Cells accumulate at these so-called checkpoints because the activity of the proteins that regulate these transitions (cyclin-dependent kinases) decreases.[55] G1 checkpoint checks several aspects of the cells such as the size, nutrients and DNA damage before entering in the replication phase, and G2 checkpoint is focused on analysing DNA damage after the replication and replication completeness. So, depending when the DNA damage occurs the cells will be arrested in different phases. Previous results have shown that mild heat shock provokes a cell-cycle arrest in the G2/M phase.[56]

Cell cycle analysis of the control 3D cell culture has revealed that around 40% of cells are in the G2M phase in both models. This phase includes both cells undergoing the G2 phase, where cells prepare themself for mitosis, and also those cells that are dividing (M phase).[57] The observation of an important percentage of cells in this sub-phase suggests a normal replication of the cells after the 3D model construction. In contrast, the analysis of the cell cycle from the cells that remained alive 24 h after the MH treatment for both models has revealed a significant decrease on the percentage of cells in the G2M and S phases, accompanied by an increase on the percentage of cells in the G0/G1 phase. These results indicate an arrest of the cells in the G0/G1 phase that does not allow the cells to duplicate its DNA and undergo the mitosis process. Therefore, it can be concluded that cells are suffering damages that are being detected by the key proteins preventing the cell replication process. The arrest is however more pronounced for the *In Model*. This result is probably a consequence of the heterogeneous distribution of MNPs along the 3D structure of the *In&Out Model* when the AMF is applied, as the core of the 3D cell culture would probably contain cells that have not incorporated MNPs or that are far away from other extracellular MNPs that act as heating agents. However, in order to have a more detailed explanation of the mechanisms involved, further experiments on the expression and activity of some proteins such as p-53 and some cyclin-dependent kinases should be performed in future studies.

It should also be briefly discussed that a small decrease in the percentage of cells in mitosis phase is observed in the *In Model* in comparison with the *In&Out Model*. This effect has been observed both in the model with cells incubated with MNPs and the control incubated without MNPs and is probably due to the protocol of the 3D model preparation. In the *In Model*, the cells have been maintained in suspension during 1 hour for the incubation period. As RAW–264.7 are adherent cells, the suspension step is less favourable for the normal cell development in comparison with the *In&Out Model*, where the cells are directly located into the collagen matrix.

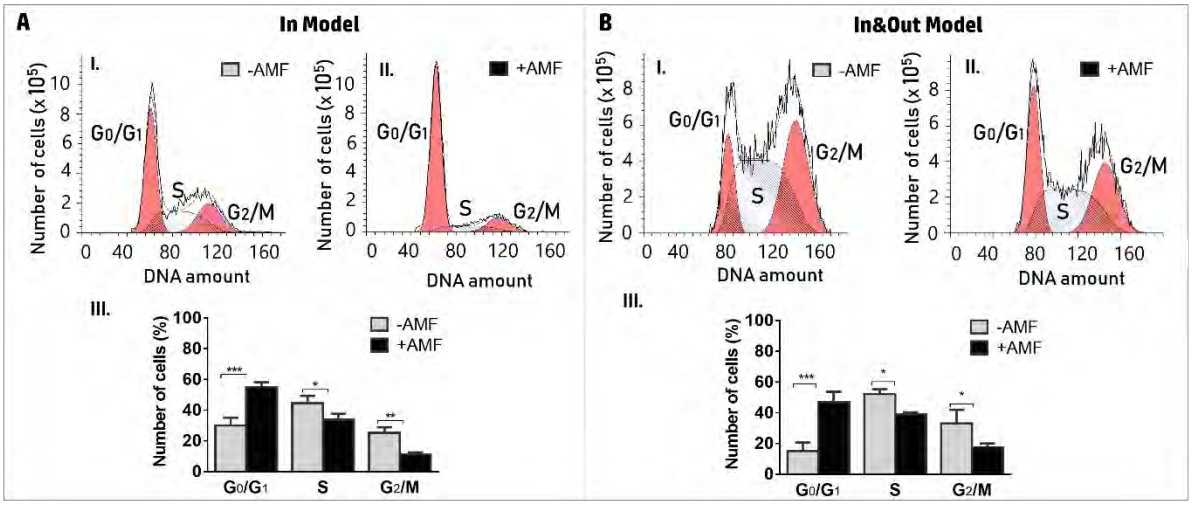

Fig. 8. ***Effect on cell cycle distribution 24 h after magnetic hyperthermia treatment.*** *(A) In Model (B) In&Out Model. The distribution of cells in each phase is given in the case of no MH treatment (I); after MH treatment (II) and the comparison of both experiments (III). Results are represented as average ± S.D. and are based on three independent experiments. Statistical significance was determined using a one-way ANOVA with Bonferroni post-test (***p<0.001; **p<0.01; *p<0.05).*

To further evaluate the effects of the cell cycle arrest observed 24 h, the experiment was extended and the number of dead cells was determined by flow cytometry up to 48 h after the MH treatment for both models. A significant decrease on the number of cells alive is observed in both models at 48 h, presenting only ≈ 4% viability (Fig. 9). Despite the fact that different cell death routes are followed, these results indicate that the hyperthermia treatment is able to kill most of the cells just 48 h after the treatment.

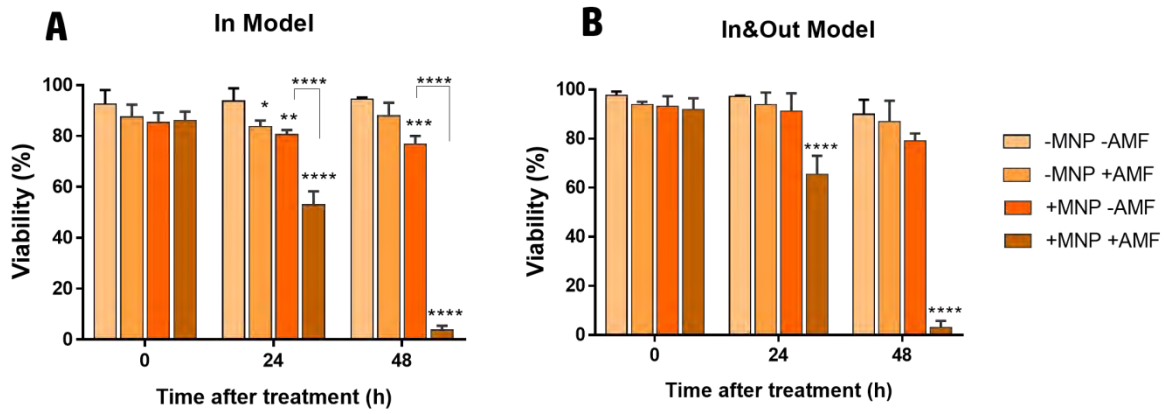

Fig. 9. ***MNPs cell viability evaluated in 3D models at different times after the Magnetic Hyperthermia treatment****. (A) In Model and (B) In&Out Model. Cell viability has been evaluated by Flow Cytometry for the two models and compared different controls: with (+MNPs) or without (-MNPs) magnetic nanoparticles, and with (+AMF) or without (-AMF) exposure to the magnetic field. Results from five independent experiments are shown as mean ± SD. Statistical significance between the means respect to the control (-MNP -AMF) was determined using a two-way ANOVA with Dunnett's multiple comparisons test (****p<0.0001; ***p<0.001; **p<0.01; *p≤0.05; p>0.05 no significance). In cases where more than one group generated significant differences with respect to control, the means between those groups were also compared.*

Magnetic Hyperthermia treatment induces different cell death mechanisms depending on the intracellular amount of MNPs. An important factor to take into account in the discussion of the previously shown results is that although the cells from both models have been incubated with the same amount of MNPs, due to the way the 3D models are prepared, cells from the *In Model* end up incorporating a higher amount of MNPs. To evaluate the amount of MNPs uptaken by the cells in both models, cells have been removed from the collagen structure and their iron content has been quantified (Table. S2, Supporting Information). When administering 100 μg of iron to both models, the intracellular iron content has been determined to be 10-fold higher for the *In Model* (8.7×10^{-8} mg Fe/cell) in comparison with the *In&Out Model* (8.1×10^{-9} mg Fe/cell) (see Fig. 10). This difference has been also verified after performing a magnetic characterization of the 3D cell cultures (See Fig. S4, Supporting Information).

It is important to highlight that these values of iron uptake confirm the high amount of MNPs that macrophages are able to internalize (depending on the incubation conditions). It is also worth mentioning that the amount of internalized MNPs in the *In&Out Model* is of the same order as the observed in other cell lines [58-59] validating the interest of our model as a tool to better understand the cellular mechanisms triggered after the AMF exposure.

Several 3D cell cultures of the *In Model* have been prepared using decreasing amounts of MNPs to assess the iron amount internalized by the cells (Fig. 10). Our findings show that it is necessary to decrease 10 times the amount of iron added to the cells in the In Model in order to achieve an intracellular amount of MNPs of the same order of magnitude (1.8×10^{-8} mg Fe/cell) as for the *In&Out Model* (Fig. 10) prepared with the highest MNPs concentration. In order to evaluate the effect of the iron content on the cell death mechanism in the *In Model*, macrophages incubated with 10 times less MNPs than in the previous experiments have been placed in a 3D matrix (*In Model-lowFe*) and exposed to the AMF. In such scenario, 24 hours after the treatment, 50% of the cells are undergoing an early apoptotic death, 35% of cells are in a late apoptosis/necrosis stage and 15% of cells remain alive (Fig. 10). These results indicate a strong influence of the MNP concentration inside the cells on the cell death mechanism triggered by the MH treatment, as a higher MNP concentration triggers a necrotic pathway (Fig. 7) while the lower MNP concentration triggers an apoptotic pathway.

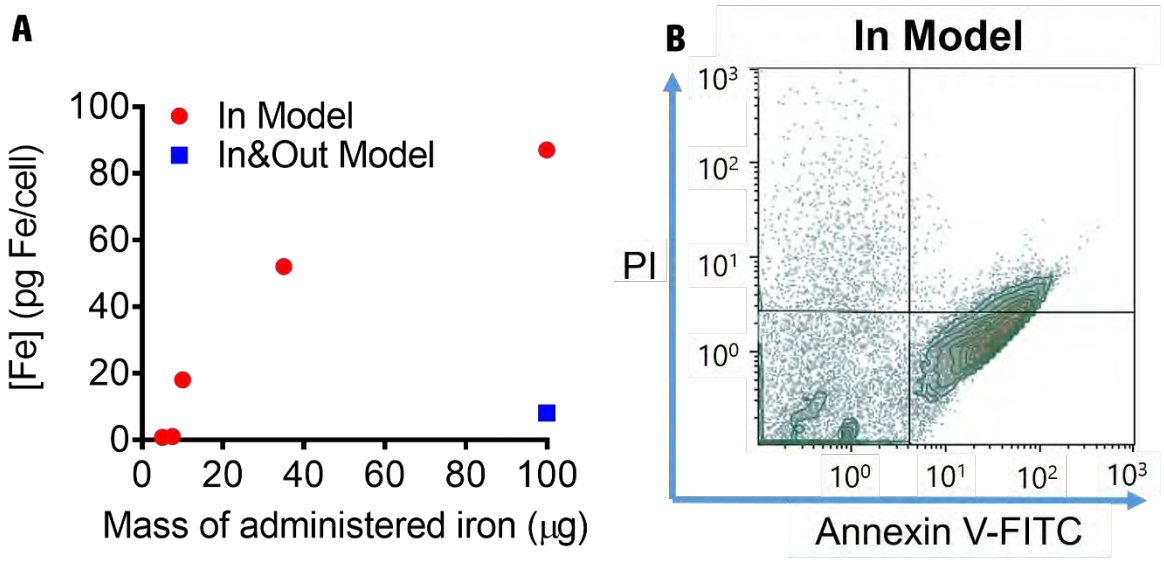

Fig. 10. ***Effect of the iron concentration inside the cells.*** *(A) Intracellular iron content for both 3D models as a function of the administered iron amount. (B) Flow cytometry analysis of the cells in the In Model-lowFe (incubated with 10 times less MNPs) 24 h after MH treatment.*

It is important to highlight that the amount of MNPs internalized by the cells is able to modulate the cell death mechanism after the exposure to an AMF. However, we are still far from the complete control of the treatment. Some studies that compare the heating capacity of different MNPs when they are either in suspension or inside the cells, have shown a clear reduction of the SAR values when the MNPs are located in cellular vesicles.[60] However, a non-monotonic relationship between MNP concentration and their heating capacity has been recently described.[61] The MNPs heating performance as a function of their packing density is a complex scenario where several factors (interactions,[61] viscosity of the medium,[62] collective behaviour, etc.) are responsible of causing either an increase or a decrease of the MNP heating capacity when decreasing the MNP concentration. Given that determining the local concentration produced as a result of the strong agglomeration of the MNPs within the cell is a complicated task, it is difficult to make predictions about the impact of the different doses on the resulting heating effects for an specific kind of material.

To evaluate the effect of such possible differences of the MNPs aggregation could have on their heating capacities, and therefore on the cell death mechanism triggered, the magnetic properties of both 3D models prepared with the higher concentration of MNPs have been measured, prior to any AMF exposure. The AC magnetic susceptibility in the 10–200 K temperature range has been measured for both models as this kind of measurements is able to detect the effect of dipolar interactions caused by local aggregation (when particles are closely packed, interparticle distances decrease and the dipolar interactions among particles increase).[63] Both samples display the characteristic features of the presence of superparamagnetic particles with a maximum in the in-phase susceptibility maxima accompanied by an out-of-phase susceptibility maximum at slightly lower temperatures.[64] The temperature dependence of the out-of-phase susceptibility, χ'' (T), shows a maximum located at slightly different temperatures for both models (Fig. 11). Still, the differences observed in these two models do not justify a significant different MNP aggregation degree that could lead to different heating properties.[61] These results are in agreement with previous studies evaluating the aggregation of MNPs in macrophage models that had shown negligible dipolar interactions among particles even during intracellular MNP aggregation.[46]

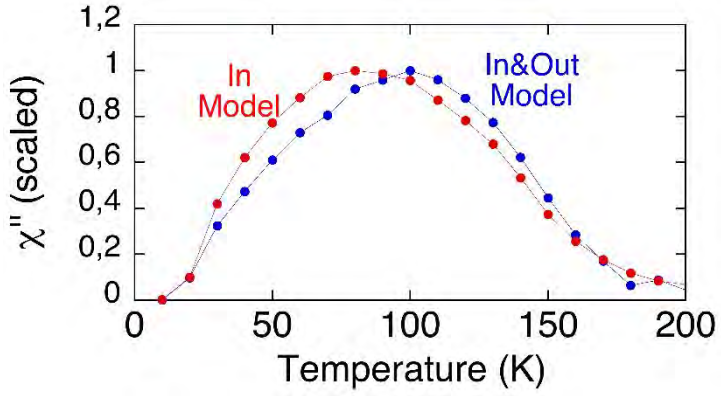

Fig. 11. ***Magnetic characterization of the 3D cell cultures****. Temperature dependence of the out-of-phase susceptibility scaled to their maximum of the two different models.*

The heterogeneous distribution of the magnetic nanoparticles within the 3D structure affects the rate of cell death. To evaluate the importance of the model on the MH treatment effect, the cell death rate observed for the *In Model-lowFe* has been compared with the *In&Out Model* (having a similar amount of internalized MNPs). In such scenario, although in both cases an apoptotic cell death mechanism is triggered, the rate of cell death is higher for the *In Model-lowFe* than for the *In&Out Model*. This is probably a consequence of the heterogeneous distribution of the MNPs amongst all the cells. It has been previously shown that, in the *In&Out Model* before the AMF exposure most of the MNPs are located at the outer areas of the 3D collagen structure (Fig. 6) and a significant number of cells do not contain any MNPs (Fig. 4). Therefore, only those cells containing MNPs and/or located in the outer areas of the 3D structure would feel the effect of the temperature increase, leading to a slower death rate. From all these results we can conclude that, even with a similar average amount of iron per cell, both models respond differently to the AMF exposure because of the initial location of the MNPs within the 3D structure.

These results highlight the importance of the development of 3D cell culture models that mimic the complex scenario of a tissue with inhomogeneous MNPs distributions. It can be foreseen that the results from studies in 2D cell cultures are probably providing misleading results that do not relate to the effect of the hyperthermia treatment as a consequence of the different incorporation of the MNPs by the cells. Furthermore, our results indicate that repetitions of the AMF exposure, once the MNPs are more homogeneously distributed throughout the 3D structure, or a delay between the MNPs administration and the AMF

application to achieve a better distribution of the particles may result in a more effective treatment *in vivo*.

Conclusions

We have prepared two different 3D cell models using a collagen matrix to mimic different possible tumour scenarios. In both models, cells have been exposed to the same amount of nanoparticles, however, while in the *In Model*, the MNPs are only located inside the cells and homogeneously distributed amongst all of them, in the *In&Out Model* a heterogeneous distribution is achieved with particles heterogeneously distributed outside the cells and also cells with and without MNPs.

The time dependence of the MNP uptake on the *In&Out Model* has been evaluated. At the initial time point, most of the MNPs are located in the outer areas of the 3D structure and therefore not all the cells have incorporated MNPs. Then, after 24h, all the cells from the 3D cell culture show the presence of MNPs inside their cytoplasm. In addition, it has been observed that this process of MNP uptake with time is faster after the exposure to the alternating magnetic field. These results are crucial for the design of *in vivo* hyperthermia treatments, as a delay between the MNP administration and the AMF exposure, or repeated cycles of AMF exposure, may improve the treatment effectiveness.

Our results demonstrate that MH induces the change in the collagen matrix that results in a more homogeneous distribution of the particles within the 3D cell culture. This observation may be of great relevance to use magnetic hyperthermia as a tool to disrupt the tumours extracellular matrix and improve the effect of other cancer treatments that have limitations to cross this barrier.

The development of these two different 3D models has allowed us to evaluate the effect of the nanoparticles concentration on the cell death mechanisms after the AMF exposure. In the *In Model*, that contains a higher amount of internalized MNPs, the main cell death mechanism observed 24 h after the MH treatment is necrosis, while in the *In&Out Model* and the *In Model-Low Fe* (containing a similar amount of MNPs as the *In&Out Model*) only apoptosis is observed at the same time point.

We have proved that the way MNPs are administered to the tumour area has a strong impact on the cell death mechanisms activated after the application of an AMF. MNPs administration route affects both the nanoparticle location within the 3D structure and concentration inside the cells and the accurate control of these two parameters is fundamental to develop an efficient and safe hyperthermia cancer treatment.

We believe that the development of these two 3D models, will have a strong impact in the study of other therapies based on magnetic nanoparticles, such as their use in photothermal therapies using laser sources.[60] However, several aspects such as the depth of the light penetration need to be optimized before.

Methods

Magnetic nanoparticle synthesis, functionalization and characterization

Iron oxide MNPs were synthesized by thermal decomposition in organic media based on a previously reported seed-mediated growth method[65] using iron (III) acetylacetonate ($Fe(acac)_3$) as a precursor.[44] This procedure rendered oleic-acid coated hydrophobic MNPs that were then transferred to water using a protocol based on the conjugation of the oleic acid with a hydrophilic polymer (poly(maleic anhydride-alt-1-octadecene, PMAO, MW 30000–50000 Da) modified with TAMRA (tetramethylrhodamine 5(6)-carboxamide cadaverine (Anaspec, Seraing, Belgium), a fluorophore that allows the *in vitro* tracking of the MNPs.[44]

Then, the coated MNPs were functionalized with glucose to provide further stability in biological media. The coated nanoparticles (1 mg of iron) were incubated with 42 μmol of N-(3-dimethylaminopropyl)-N'-ethylcarbodiimide hydrochloride (EDC) and 30 μmol of 4-aminophenyl β-D-glucopyranoside in 250 μL of SSB buffer (50 mM of boric acid and 50 mM of sodium borate) at pH 9. After 3 h at room temperature, the excess of reagents was removed by washing the sample with phosphate-buffered saline buffer (PBS) at pH 7.4 in a centrifugal filter.[2] Finally, nanoparticles were passed through syringe filters with a pore size of 0.22 μm (Merck Millipore, Darmstadt, Germany).

Dynamic light scattering and ζ-potential measurements were performed in water and in complete Dulbecco's Modified Eagle's Medium GlutaMAX™ Supplement (cDMEM; Gibco®, Thermo Fisher Scientific) on a Malvern Zetasizer Nano-ZS, using ten runs per measurement and five replicates at 25 °C and pH 7.

Particle size and morphology were studied by Transmission Electron Microscopy (TEM) using a Tecnai T20 (FEI company, OR, USA) microscope operating at 200 kV. The sample was prepared by placing a drop of a diluted suspension of the MNPs in water onto a carbon-coated grid and allowing it to dry. Particle size was determined by manual measurement of 200 particles using the Digital Micrograph software.

The heating capacity of the MNPs was determined using a commercial Alternating Magnetic Field generator (DM100; Nanoscale Biomagnetics, Spain). A 1 mg Fe/mL MNP sample was placed in a closed container centred in the inductive coil. The AMF was applied for 5 min using a field amplitude of H = 20 kA/m, and a frequency of 829 kHz while the temperature was recorded using an optic fiber sensor incorporated in the equipment.

For the magnetic characterization, the MNPs liquid sample was allowed to dry at room temperature deposited into a piece of cotton wool that was subsequently placed into a gelatine capsule. Field dependent magnetization measurements were performed in a Quantum Design (USA) MPMS-XL SQUID magnetometer at 300 K with a maximum field of 5 T.

Sterility assay

Swab and Samplers Test Kits (Merck Millipore) were used for the quality control of the MNPs sterility. The microbiological analysis aimed at detecting bioburden levels of bacteria, yeast or mold (Coli-Count™, Heterotrophic Plate Count and Yeast and Mold Samplers). The MNPs were tested in the sampler membrane, covered with growth medium for specific microorganism, at the common dilution used for the *in vitro* studies following the incubation conditions specified by the manufacturer (Coli-Count 35 °C, 22-24 h; Yeast and Mold 28-32 °C, 48-72 h; Heterotrophic Plate Count (HPC) Sampler 25-35 °C, 48-72h). After the incubation, the filter surface was examined with an illuminator to identify the presence of microbial colonies.

Cell line

The murine macrophage RAW–264.7 cell line (ATCC® TIB71™) was cultured and maintained in cDMEM supplemented with 10 % fetal bovine serum (FBS, Invitrogen), 100 U/mL penicillin G (sodium salt) and 100 μg/mL streptomycin sulfate (Invitrogen) at 37 °C in a humidified atmosphere at 5 % CO_2. To detach the cells, a two-step protocol was followed trying to enhance the cells viability. First, cells were incubated with Trypsin EDTA solution (Sigma Aldrich) for 5 minutes at 37 ºC and then, the cells were scrapped from the flask. Finally cells were collected in fresh cDMEM.

Formation of 3D cell culture models

3D cell culture gels were prepared as follows. First, 250 μL of a $4x10^6$ cells/mL suspension in complete culture medium were mixed with fetal bovine serum (Invitrogen) and Modified Eagle's Medium 10x (MEM w/Earle´s salts, w/o Glutamine, w/o Sodium Bicarbonate, First Link UK Ltd) in a 1:1:1 volumetric ratio. The resulting cell suspension was added to an ice-cold mixture of 1.25 mL rat tail Collagen type I (Protein concentration 2.05 mg/mL in 0.6 % acetic acid, First Link UK Ltd) solution and 0.5 mL 0,1 % sodium hydroxide (NaOH)

solution. Then, some drops of NaOH were added while gently shaking until the medium turned pink. After that, the final mixture was added quickly to a 24 well plate (600 μL / well, ≈ 10^6 cells / well, Thermo Scientific Nunc Cell-Culture) and incubated at 37 °C for 30 min. After collagen gellification, 0.5 mL of complete culture medium was added per gel.

Two different strategies for the incubation with magnetic nanoparticles were followed. The first model where nanoparticles are located only inside the cells - In Model- was prepared by incubating detached cells ($4x10^6$ cells/mL in complete medium) with the MNPs (0.2 mgFe/mL) during 1 h at 37 ºC and then washing the particles that had not been uptaken by centrifugation (161 rcf, 6 min) twice. After that, the cells were used to form the collagen gel.

The second strategy produced the 3D cell culture where the particles are located both inside and outside the cells - In&Out Model, and also have a heterogeneous localization within the 3D structure. To achieve this, the 3D model containing the cells was formed as described before. Just after collagen solidification, 500 μL of a MNP solution of 0.2 mg Fe/mL in complete medium were added and incubated at 37 °C for 1 h. After that, the supernatant was removed, the 3D cell culture was washed twice, and 500 μL of complete culture medium were added to the 3D model.

MNPs toxicity.

2D cell cultures were incubated during 1 h with increasing amounts of iron (10, 20 50, 100 and 200 μg) prepared in a final volume of 500 μL. 3D cell cultures were incubated with 100 μg of iron during 1 h. Cell viability was assessed by flow cytometry.

Magnetic Hyperthermia treatment

Before starting the AMF exposure and during the treatment, 3D cell cultures were thermalized at 37 °C using a water bath pump (Stryker - Medical Devices & Equipment Manufacturing Company) connected to a water tubing jacket. Then, the 3D cell cultures were exposed to an AMF during 30 min at a frequency of 377.5 kHz and field amplitude of 13 kAm^{-1} using a commercial AMF generator (DM3, nB nanoscale Biomagnetics, Zaragoza, Spain).

Flow cytometry studies

Cells were released from the 3D cell cultures using a treatment with collagenase type I (isolated from *Cl. histolyticum* lyophilized, non-sterile, Gibco™ Thermo Fisher Scientific) at 2 mg/mL in HBSS (Hank's Balanced Salt Solution) during 30 min at 37 ºC. Then, cells were washed by centrifugation (161 rcf, 6 min) and re-suspended in PBS (Phosphate Buffer Saline pH=7.4). All samples were analysed in a Gallios™ Flow Cytometer (Beckman Coulter) and the data interpreted with Kaluza 1.5a Software (Beckman Coulter).

To determine the MNPs uptake, cells re-suspended in PBS at a concentration of $2.5x10^4$ cells/mL were analysed by flow cytometry.

To study the cell viability, cells were re-suspended in 1X Annexin V Binding Buffer (10 mM Hepes/NaOH (pH=7.4) 140 mM NaCl, 2,5 mM $CaCl_2$) at a concentration of 10^6 cells/mL. Then, 5 µl of the Annexin V-FITC (Fluorescein Isothiocyanate) and 5 µL of Propidium Iodide (PI) were added to 100 µL of cell suspension and incubated at room temperature for 15 minutes in the dark (FITC-Annexin V Apoptosis Detection Kit). After the incubation period, 400 µL of 1X Annexin binding buffer was added and the sample was analysed by flow cytometry.

To evaluate the cell cycle, cells were fixed with cold ethanol (70%) during 24 h and, after that, incubated with propidium iodide during 30 min in dark for analysis by flow cytometry. The data obtained was treated with the MODFIT LT 3.0 Verity Software (G0/G1, G2/M and S indicate the cell cycle phase while sub-G0/G1 refers to the proportion of apoptotic cells.)

Confocal microscopy

To study the MNP internalization, the 3D cell cultures were fixed during 20 min with 500 µL of paraformaldehyde (4%). Then, the nuclei were stained with DAPI (4′,6-diamidino-2-phenylindole) and the cytoskeleton with Phalloidin488. An Olympus FV10i Confocal Laser Scanning Microscope equipped with 405 nm (18 mW), 473 nm (12.5 mW) and 635 nm (10 mW) lasers was used to acquire images of the cells. The images were then processed using Olympus Fluoview FV10-ASW 3.1 Viewer software (Olympus Canada, Markham, ON, Canada). The three dimensional projection images of the 3D cell cultures were obtained with a Zeiss LSM 880 Confocal Microscope with a 63x/1.40 Plan Apochromat objective. The laser sources used were 458 nm, 488 nm (Argon Ion), 561 nm (DPSS- Diode-pumped solid state). ZEN Microscope and Imaging Software were used for the image analysis.

Magnetic characterization

3D cell cultures were freeze-dried and placed into gelatine capsules for their magnetic characterization. AC (alternating current) magnetic susceptibility measurements were performed in a Quantum Design (USA) MPMS-XL SQUID magnetometer with an AC amplitude of 0.41 Oe, in the temperature range between 10 and 200 K and at a frequency of 11 Hz.

Iron quantification

Iron concentration was determined using a standard colorimetric procedure.[66] For the MNPs, an aliquot was digested with aqua regia for 15 min at 60 °C and diluted with Milli-Q water.

For the cells, 3D cell cultures were treated with collagenase (2 mg/mL) 30 min at 37 °C and after that the cells were spun down in a mini spin centrifuge. The digestion of the cells was performed heating with HNO_3 (Panreac) and then with H_2O_2 (Panreac) (both steps at 90ºC and during 1 h each). A calibration curve was prepared by dilution of an Iron standard solution 1 mg/mL Fe in 2% HNO_3 (Acros Organics, USA). The digested samples were incubated at room temperature for 15 min after the addition of KOH (4 N), 4,5-dihydroxy-1,3-benzenedisulfonic acid disodium salt monohydrate (Tiron) and sodium phosphate buffer (0.2 M pH=9.7). Finally, sample absorbance (480 nm) was measured on an UV/Vis spectrophotometer (Thermo Scientific Multiskan™ GO MA, USA) and compared to a calibration curve.

Statistical analysis

Data are expressed as mean ± SD of a minimum three biological replicas. Statistical significance of difference in means was performed using GraphPad Prism v7.00 Student´s test and one-way ANOVA test were used for the analysis of the data. The confidence interval was 95%. Bonferroni post-test was used to determine which means differed.

Associated content

Complementary results are supplied as Supporting Information*:*

Table S1. Hydrodynamic size and ζ – potential of magnetic nanoparticles.

Table. S2. Iron concentration located inside the cells.

Fig. S1. Sterility assay.

Fig. S2. MNPs toxicity assay in 2D cell cultures.

Fig. S3. MNPs toxicity evaluated in 3D models.

Fig. S4. Magnetic characterization of the 3D models.

Author information

Acknowledgment

The present work was supported by grants from the Universidad de Zaragoza (UZ2018-CIE-03), Spanish MINECO (MAT2011-26851-CO2-01, SAF2014-54763-C2-2-R and BIO2017-84246-C2-1-R), Fondo Social de la DGA (grupos DGA), COST Action TD1402 (Radiomag), and the European Commission through the M-ERA.NET COFUND project MagicCellGene (PCIN-2017-060).

LB thanks Santander-Universidad Zaragoza Fellowship program for her PhD position. L.A acknowledges financial support from the Juan de la Cierva program (JFC1-2014-20655). R L.G. and R.M.F. acknowledge financial support from the Ramón y Cajal subprogram (RYC-2014-15512 and RYC-2015-17640). Authors would like to acknowledge the use of Servicios Científicos Técnicos del CIBA (IACS-Universidad de Zaragoza), the Advanced Microscopy Laboratory (INA-Universidad de Zaragoza) for access to their instrumentation and expertise and Servicio General de Apoyo a la Investigación-SAI, Universidad de Zaragoza.

References

1. Colombo, M.; Carregal-Romero, S.; Casula, M. F.; Gutierrez, L.; Morales, M. P.; Bohm, I. B.; Heverhagen, J. T.; Prosperi, D.; Parak, W. J., Biological Applications of Magnetic Nanoparticles. *Chem. Soc. Rev.* **2012,** *41* (11), 4306-4334.
2. Moros, M.; Pelaz, B.; Lopez-Larrubia, P.; Garcia-Martin, M. L.; Grazu, V.; de la Fuente, J. M., Engineering Biofunctional Magnetic Nanoparticles for Biotechnological Applications. *Nanoscale* **2010,** *2* (9), 1746-1755.
3. Eifler, A. C.; Thaxton, C. S., Nanoparticle Therapeutics: Fda Approval, Clinical Trials, Regulatory Pathways, and Case Study. *Methods Mol. Biol.* **2011,** *726*, 325-338.
4. Jain, K. K., Advances in the Field of Nanooncology. *BMC Med* **2010,** *8*, 83.
5. Perez-Lopez, B.; Merkoci, A., Nanoparticles for the Development of Improved (Bio)Sensing Systems. *Anal. Bioanal. Chem.* **2011,** *399* (4), 1577-1590.
6. Arruebo, M.; Fernández-Pacheco, R.; Ibarra, R. M.; Santamaría, J., Magnetic Nanoparticles for Drug Delivery. *Nano Today* **2007,** *2* (3), 22-32.
7. Neuberger, T.; Schöpf, B.; Hofmann, H.; Hofmann, M.; von Rechenberg, B., Superparamagnetic Nanoparticles for Biomedical Applications: Possibilities and Limitations of a New Drug Delivery System. *J. Magn. Magn. Matter.* **2005,** *293* (1), 483-496.
8. Rosen, J. E.; Chan, L.; Shieh, D. B.; Gu, F. X., Iron Oxide Nanoparticles for Targeted Cancer Imaging and Diagnostics. *Nanomedicine* **2012,** *8* (3), 275-290.
9. Huh, Y. M.; Jun, Y. W.; Song, H. T.; Kim, S.; Choi, J. S.; Lee, J. H.; Kim, K. S.; Shin, J. S.; Suh, J. S.; Cheon, J., In Vivo Magnetic Resonance Detection of Cancer by Using Multifunctional Magnetic Nanocrystals. *J. Am. Chem. Soc.* **2005,** *127*, 12387-12391.
10. Jordan, A.; Scholz, R.; Wust, P.; Fähling, H.; Roland, F., Magnetic Fluid Hyperthermia (Mfh): Cancer Treatment with Ac Magnetic Field Induced Excitation of Biocompatible Superparamagnetic Nanoparticles. *J. Magn. Magn. Matter.* **1999,** *201* (1–3), 413-419.
11. Beik, J.; Abed, Z.; Ghoreishi, F. S.; Hosseini-Nami, S.; Mehrzadi, S.; Shakeri-Zadeh, A.; Kamrava, S. K., Nanotechnology in Hyperthermia Cancer Therapy: From Fundamental Principles to Advanced Applications. *J. Control Release* **2016,** *235*, 205-221.
12. Wust, P.; Hildebrandt, B.; Sreenivasa, G.; Rau, B.; Gellermann, J.; Riess, H.; Felix, R.; Schlag, P. M., Hyperthermia in Combined Treatment of Cancer. *Lancet. Oncol.* **2002,** *3* (8), 487-497.
13. Banobre-Lopez, M.; Teijeiro, A.; Rivas, J., Magnetic Nanoparticle-Based Hyperthermia for Cancer Treatment. *Rep. Pract. Oncol. Radiother.* **2013,** *18* (6), 397-400.
14. Kobayashi, T., Cancer Hyperthermia Using Magnetic Nanoparticles. *Biotechnol. J.* **2011,** *6* (11), 1342-1347.

15. Laurent, S.; Dutz, S.; Häfeli, U. O.; Mahmoudi, M., Magnetic Fluid Hyperthermia: Focus on Superparamagnetic Iron Oxide Nanoparticles. *Adv. Colloid. and Interfac. Sci.* **2011,** *166* (1), 8-23.
16. Hildebrandt, B.; Wust, P.; Ahlers, O.; Dieing, A.; Sreenivasa, G.; Kerner, T.; Felix, R.; Riess, H., The Cellular and Molecular Basis of Hyperthermia. *Crit. Rev. Oncol. Hematol.***2002,** *43* (1), 33-56.
17. Ohtake, M.; Umemura, M.; Sato, I.; Akimoto, T.; Oda, K.; Nagasako, A.; Kim, J.-H.; Fujita, T.; Yokoyama, U.; Nakayama, T.; Hoshino, Y.; Ishiba, M.; Tokura, S.; Hara, M.; Muramoto, T.; Yamada, S.; Masuda, T.; Aoki, I.; Takemura, Y.; Murata, H.; Eguchi, H.; Kawahara, N.; Ishikawa, Y., Hyperthermia and Chemotherapy Using Fe(Salen) Nanoparticles Might Impact Glioblastoma Treatment. *Sci. Rep.* **2017,** *7*, 42783.
18. Sato, I., Simultaneous Hyperthermia-Chemotherapy with Controlled Drug Delivery Using Single-Drug Nanoparticles. *Sci. Rep.* **2016,** *6*, 24629.
19. Thorat, N. D.; Bohara, R.; Yadav, H. M.; Otari, S. V.; Pawar, S. H.; Tofail, S. A. M., Multifunctional Magnetic Nanostructures for Cancer Hyperthermia Therapy. Book: "*Nanoarchitectonics for Smart Delivery and Drug Targeting*" **2016**, 589-612.
20. Krawczyk, P. M.; Eppink, B.; Essers, J.; Stap, J.; Rodermond, H.; Odijk, H.; Zelensky, A.; van Bree, C.; Stalpers, L. J.; Buist, M. R., Mild Hyperthermia Inhibits Homologous Recombination, Induces Brca2 Degradation, and Sensitizes Cancer Cells to Poly (Adp-Ribose) Polymerase-1 Inhibition. *Proc. Natl. Acad. Sci. U S A* **2011,** *108* (24), 9851-9856.
21. Grivennikov, S. I.; Greten, F. R.; Karin, M., Immunity, Inflammation, and Cancer. *Cell* **2010,** *140* (6), 883-899.
22. Berghe, T. V.; Linkermann, A.; Jouan-Lanhouet, S.; Walczak, H.; Vandenabeele, P., Regulated Necrosis: The Expanding Network of Non-Apoptotic Cell Death Pathways. *Nat. Rev. Mol. Cell Biol.* **2014,** *15* (2), 135-147.
23. Krysko, D. V.; Garg, A. D.; Kaczmarek, A.; Krysko, O.; Agostinis, P.; Vandenabeele, P., Immunogenic Cell Death and Damps in Cancer Therapy. *Nat. Rev. Cancer* **2012,** *12* (12), 860-875.
24. Sanz, B.; Calatayud, M. P.; Torres, T. E.; Fanarraga, M. L.; Ibarra, M. R.; Goya, G. F., Magnetic Hyperthermia Enhances Cell Toxicity with Respect to Exogenous Heating. *Biomaterials* **2017,** *114*, 62-70.
25. Patil, R. M.; Thorat, N. D.; Shete, P. B.; Otari, S. V.; Tiwale, B. M.; Pawar, S. H., In Vitro Hyperthermia with Improved Colloidal Stability and Enhanced Sar of Magnetic Core/Shell Nanostructures. *Mater Sci Eng C Mater Biol Appl* **2016,** *59*, 702-709.
26. Calatayud, M. P.; Soler, E.; Torres, T. E.; Campos-Gonzalez, E.; Junquera, C.; Ibarra, M. R.; Goya, G. F., Cell Damage Produced by Magnetic Fluid Hyperthermia on Microglial Bv2 Cells. *Sci. Rep.* **2017,** *7* (1), 8627.
27. Justice, B. A.; Badr, N. A.; Felder, R. A., 3d Cell Culture Opens New Dimensions in Cell-Based Assays. *Drug. Discov. Today* **2009,** *14* (1-2), 102-107.
28. Lee, J.; Cuddihy, M. J.; Kotov, N. A., Three-Dimensional Cell Culture Matrices: State of the Art. *Tissue. Eng. Part. B Rev.* **2008,** *14* (1), 61-86.
29. McHale, G.; Newton, M., Liquid Marbles: Topical Context within Soft Matter and Recent Progress. *Soft. Matter.* **2015,** *11* (13), 2530-2546.
30. Derda, R.; Laromaine, A.; Mammoto, A.; Tang, S. K.; Mammoto, T.; Ingber, D. E.; Whitesides, G. M., Supported 3d Cell Culture for Tissue-Based Bioassays. *Proc. Natl. Acad. Sci. U S A* **2009,** *106* (44), 18457-18462.
31. Cukierman, E.; Pankov, R.; Stevens, D. R.; Yamada, K. M., Taking Cell-Matrix Adhesions to the Third Dimension. *Science* **2001,** *294* (5547), 1708-1712.

32. Tambe, D. T.; Hardin, C. C.; Angelini, T. E.; Rajendran, K.; Park, C. Y.; Serra-Picamal, X.; Zhou, E. H.; Zaman, M. H.; Butler, J. P.; Weitz, D. A.; Fredberg, J. J.; Trepat, X., Collective Cell Guidance by Cooperative Intercellular Forces. *Nat. Mater.* **2011,** *10* (6), 469-475.
33. Pampaloni, F.; Reynaud, E. G.; Stelzer, E. H., The Third Dimension Bridges the Gap between Cell Culture and Live Tissue. *Nat. Rev. Mol. Cell Biol.* **2007,** *8* (10), 839-845.
34. Stocke, N. A.; Sethi, P.; Jyoti, A.; Chan, R.; Arnold, S. M.; Hilt, J. Z.; Upreti, M., Toxicity Evaluation of Magnetic Hyperthermia Induced by Remote Actuation of Magnetic Nanoparticles in 3d Micrometastasic Tumor Tissue Analogs for Triple Negative Breast Cancer. *Biomaterials* **2017,** *120*, 115-125.
35. van Kempen, L. C.; Ruiter, D. J.; van Muijen, G. N.; Coussens, L. M., The Tumor Microenvironment: A Critical Determinant of Neoplastic Evolution. *Eur. J. Cell Biol.* **2003,** *82* (11), 539-548.
36. Trédan, O.; Galmarini, C. M.; Patel, K.; Tannock, I. F., Drug Resistance and the Solid Tumor Microenvironment. *J. Ntl. Cancer Inst.* **2007,** *99* (19), 1441-1454.
37. Netti, P. A.; Berk, D. A.; Swartz, M. A.; Grodzinsky, A. J.; Jain, R. K., Role of Extracellular Matrix Assembly in Interstitial Transport in Solid Tumors. *Cancer Res.* **2000,** *60* (9), 2497-2503.
38. Rojas, J. M.; Sanz-Ortega, L.; Mulens-Arias, V.; Gutierrez, L.; Perez-Yague, S.; Barber, D. F., Superparamagnetic Iron Oxide Nanoparticle Uptake Alters M2 Macrophage Phenotype, Iron Metabolism, Migration and Invasion. *Nanomedicine* **2016,** *12* (4), 1127-1138.
39. L. Beola, L. G., V. Grazú, L. Asín, A Roadmap to the Standardization of in Vivo Magnetic Hyperthermia. *Elsevier Book: "Nanomaterials for Magnetic and Optical Hyperthermia Applications"*, in press.
40. Kobayashi, T.; Ito, A.; Honda, H., Magnetic Nanoparticle-Mediated Hyperthermia and Induction of Anti-Tumor Immune Responses. In *Hyperthermic Oncology from Bench to Bedside*, Kokura, S.; Yoshikawa, T.; Ohnishi, T., Eds. Springer Singapore: Singapore, 2016; pp 137-150.
41. Moros, M.; Hernáez, B.; Garet, E.; Dias, J. T.; Sáez, B.; Grazú, V.; González-Fernández, A. f.; Alonso, C.; de la Fuente, J. s. M., Monosaccharides Versus Peg-Functionalized Nps: Influence in the Cellular Uptake. *ACS nano* **2012,** *6* (2), 1565-1577.
42. Macheda, M. L.; Rogers, S.; Best, J. D., Molecular and Cellular Regulation of Glucose Transporter (Glut) Proteins in Cancer. *J. Cell. Physiol.* **2005,** *202* (3), 654-662.
43. Fratila, R. M.; Navascuez, M.; Idiago-López, J.; Eceiza, M.; Miranda, J. I.; Aizpurua, J. M.; Jesús, M., Covalent Immobilisation of Magnetic Nanoparticles on Surfaces Via Strain-Promoted Azide–Alkyne Click Chemistry. *New J. Chem.* **2017,** *41* (19), 10835-10840.
44. Stepien, G.; Moros, M.; Perez-Hernandez, M.; Monge, M.; Gutierrez, L.; Fratila, R. M.; Las Heras, M.; Menao Guillen, S.; Puente Lanzarote, J. J.; Solans, C.; Pardo, J.; de la Fuente, J. M., Effect of Surface Chemistry and Associated Protein Corona on the Long-Term Biodegradation of Iron Oxide Nanoparticles in Vivo. *ACS Appl Mater Interfaces* **2018,** *10* (5), 4548-4560.
45. Moros, M.; Ambrosone, A.; Stepien, G.; Fabozzi, F.; Marchesano, V.; Castaldi, A.; Tino, A.; de la Fuente, J. M.; Tortiglione, C., Deciphering Intracellular Events Triggered by Mild Magnetic Hyperthermia in Vitro and in Vivo. *Nanomedicine* **2015,** *10* (14), 2167-2183
46. Rojas, J. M.; Gavilan, H.; Del Dedo, V.; Lorente-Sorolla, E.; Sanz-Ortega, L.; da Silva, G. B.; Costo, R.; Perez-Yague, S.; Talelli, M.; Marciello, M.; Morales, M. P.; Barber, D. F.; Gutierrez, L., Time-Course Assessment of the Aggregation and Metabolization of Magnetic Nanoparticles. *Acta Biomater.* **2017,** *58*, 181-195.

47. Kolosnjaj-Tabi, J.; Di Corato, R.; Lartigue, L.; Marangon, I.; Guardia, P.; Silva, A. K. A.; Luciani, N.; Clément, O.; Flaud, P.; Singh, J. V.; Decuzzi, P.; Pellegrino, T.; Wilhelm, C.; Gazeau, F., Heat-Generating Iron Oxide Nanocubes: Subtle "Destructurators" of the Tumoral Microenvironment. *ACS nano* **2014,** *8* (5), 4268-4283.
48. Privalov, P. L., Stability of Proteins: Proteins Which Do Not Present a Single Cooperative System. In *Advances in Protein Chemistry*, Elsevier: 1982; Vol. 35, 1-104
49. Xia, Z.; Calderon-Colon, X.; Trexler, M.; Elisseeff, J.; Guo, Q., Thermal Denaturation of Type I Collagen Vitrified Gels. *Thermochim. Acta.* **2012,** *527*, 172-179.
50. Ioachim, E.; Charchanti, A.; Briasoulis, E.; Karavasilis, V.; Tsanou, H.; Arvanitis, D. L.; Agnantis, N. J.; Pavlidis, N., Immunohistochemical Expression of Extracellular Matrix Components Tenascin, Fibronectin, Collagen Type Iv and Laminin in Breast Cancer: Their Prognostic Value and Role in Tumour Invasion and Progression. *Eur. J. Cancer* **2002,** *38* (18), 2362-2370.
51. Stone, L., Prostate Cancer: A Glitch in the Extracellular Matrix. *Nat. Rev. Urol.* **2016,** *14* (1), 8-9.
52. Gritsenko, P.; Leenders, W.; Friedl, P., Recapitulating in Vivo-Like Plasticity of Glioma Cell Invasion Along Blood Vessels and in Astrocyte-Rich Stroma. *Histochem. Cell. Biol.* **2017,** *148* (4), 395-406.
53. Miyamoto, H.; Murakami, T.; Tsuchida, K.; Sugino, H.; Miyake, H.; Tashiro, S., Tumor-Stroma Interaction of Human Pancreatic Cancer: Acquired Resistance to Anticancer Drugs and Proliferation Regulation Is Dependent on Extracellular Matrix Proteins. *Pancreas* **2004,** *28* (1), 38-44.
54. Wlodkowic, D.; Skommer, J.; Darzynkiewicz, Z., Flow Cytometry-Based Apoptosis Detection. *Methods. Mol. Biol.* **2009,** *559*, 19-32.
55. Kühl, N. M.; Rensing, L., Heat Shock Effects on Cell Cycle Progression. *Cell. Mol. Life. Sci.* **2000,** *57* (3), 450-463.
56. Alekseenko, L. L.; Zemelko, V. I.; Domnina, A. P.; Lyublinskaya, O. G.; Zenin, V. V.; Pugovkina, N. A.; Kozhukharova, I. V.; Borodkina, A. V.; Grinchuk, T. M.; Fridlyanskaya, I. I., Sublethal Heat Shock Induces Premature Senescence Rather Than Apoptosis in Human Mesenchymal Stem Cells. *Cell Stres. Chaperon.* **2014,** *19* (3), 355-366.
57. Szüts, D.; Krude, T., Cell Cycle Arrest at the Initiation Step of Human Chromosomal DNA Replication Causes DNA Damage. *J. Cell Sci.* **2004,** *117* (21), 4897-4908.
58. Asín, L.; Ibarra, M. R.; Tres, A.; Goya, G. F., Controlled Cell Death by Magnetic Hyperthermia: Effects of Exposure Time, Field Amplitude, and Nanoparticle Concentration. *Pharm. Res.* **2012,** *29* (5), 1319-1327.
59. Ahmed, M. S. U.; Salam, A. B.; Clayton Yates, K. W.; Jaynes, J.; Turner, T.; Abdalla, M. O., Double-Receptor-Targeting Multifunctional Iron Oxide Nanoparticles Drug Delivery System for the Treatment and Imaging of Prostate Cancer. *Int. J. Nanomedicine* **2017,** *12*, 6973-6984.
60. Espinosa, A.; Kolosnjaj-Tabi, J.; Abou-Hassan, A.; Plan Sangnier, A.; Curcio, A.; Silva, A. K.; Di Corato, R.; Neveu, S.; Pellegrino, T.; Liz-Marzán, L. M., Magnetic (Hyper) Thermia or Photothermia? Progressive Comparison of Iron Oxide and Gold Nanoparticles Heating in Water, in Cells, and in Vivo. *Adv. Funct. Mater.* **2018,** *28* (37), 1803660.
61. Conde-Leboran, I.; Baldomir, D.; Martinez-Boubeta, C.; Chubykalo-Fesenko, O.; del Puerto Morales, M.; Salas, G.; Cabrera, D.; Camarero, J.; Teran, F. J.; Serantes, D., A Single Picture Explains Diversity of Hyperthermia Response of Magnetic Nanoparticles. *J. Phys. Chem. C* **2015,** *119* (27), 15698-15706.
62. Cabrera, D.; Coene, A.; Leliaert, J.; Artes-Ibanez, E. J.; Dupre, L.; Telling, N. D.; Teran, F. J., Dynamical Magnetic Response of Iron Oxide Nanoparticles inside Live Cells. *ACS Nano* **2018,** *12* (3), 2741-2752.

63. Lopez, A.; Gutierrez, L.; Lazaro, F. J., The Role of Dipolar Interaction in the Quantitative Determination of Particulate Magnetic Carriers in Biological Tissues. *Phys. Med. Biol.* **2007,** *52* (16), 5043-5056.
64. Gutiérrez, L.; Morales, M. P.; Lázaro, F. J., Prospects for Magnetic Nanoparticles in Systemic Administration: Synthesis and Quantitative Detection. *Phys. Chem. Chem. Phys.* **2014,** *16* (10), 4456-4464.
65. Sun, S.; Zeng, H.; Robinson, D. B.; Raoux, S.; Rice, P. M.; Wang, S. X.; Li, G., Monodisperse Mfe_2o_4 (M = Fe, Co, Mn) Nanoparticles. *J. Am. Chem. Soc.* **2004,** *126*, 273-279.
66. Dias, J. T.; Moros, M.; Del Pino, P.; Rivera, S.; Grazu, V.; de la Fuente, J. M., DNA as a Molecular Local Thermal Probe for the Analysis of Magnetic Hyperthermia. *Angew. Chem. Int. Ed. Engl.* **2013,** *52* (44), 11526-11529.

Table of contents:

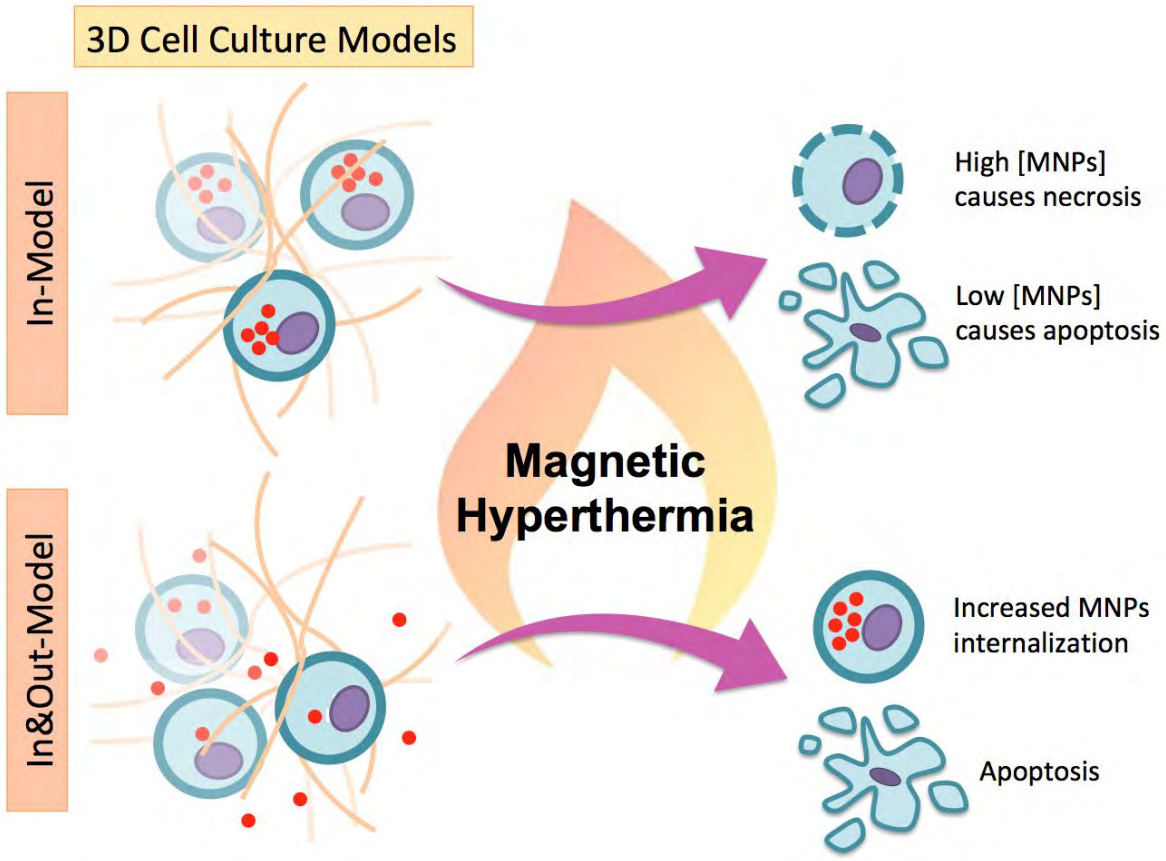

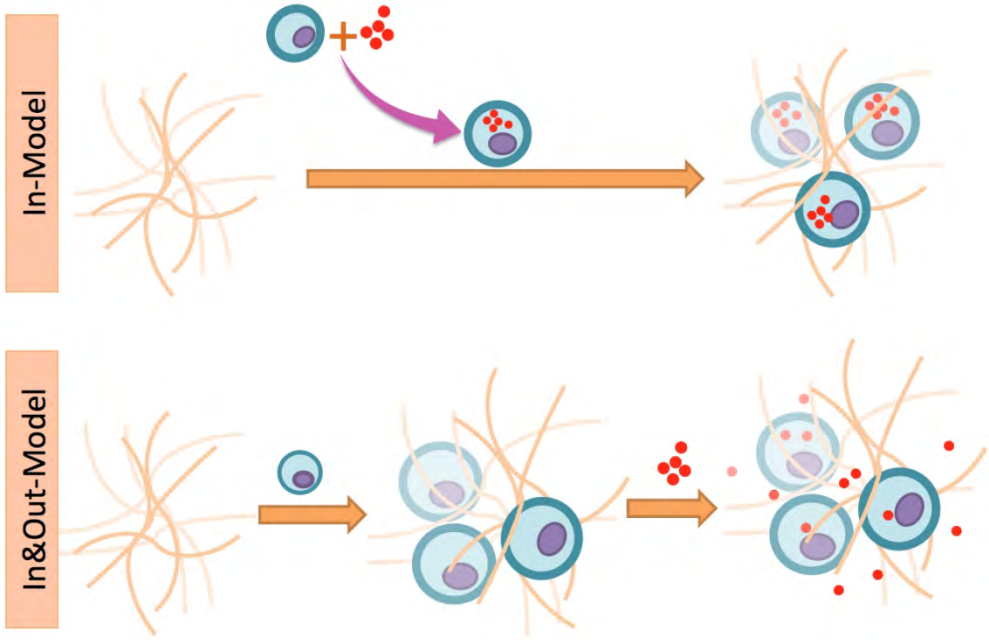

Fig. 1. Representation of the formation of the two 3D models used in this work. In Model, where the MNPs are located just inside the cells. In&Out Model, where MNPs are located both inside and outside the cells.

451x302mm (72 x 72 DPI)

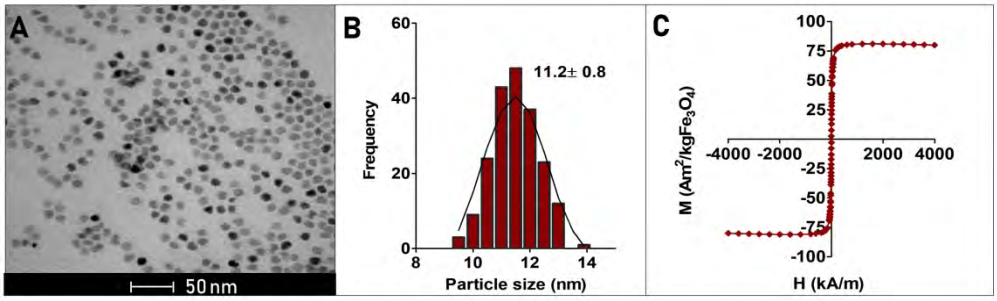

Fig. 2. Magnetic nanoparticle characterization. (A) TEM micrograph, (B) Particle size distribution analysis and (C) Field dependent magnetization of the MNPs in water.

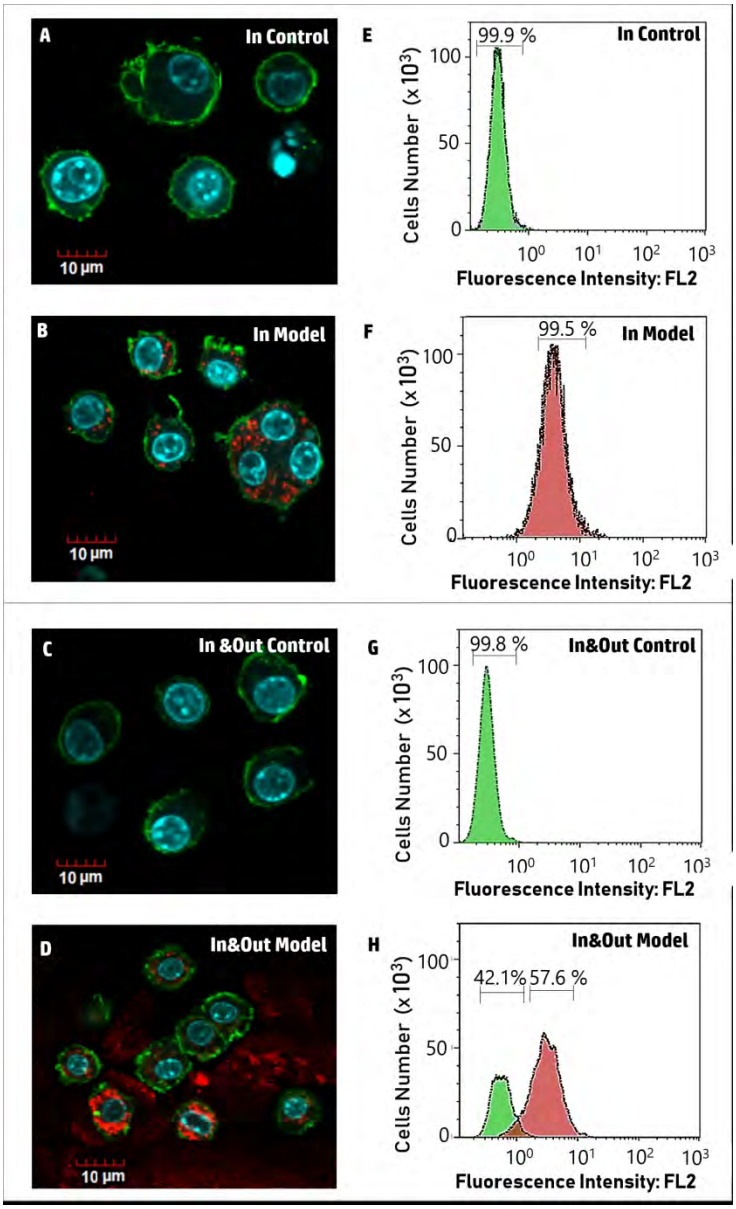

Fig. 3. 3D cell culture characterization (A, B, C, D) Confocal images. The nucleus is shown in blue (DAPI), actin in green (Phalloidin_AlexaFluor488) and MNPs in red (TAMRA). Scale bar: 10 µm. (E, F, G, H) Flow cytometry analysis of nanoparticle uptake. Data have been selected as a representation of a series of five experiments.

258x424mm (150 x 150 DPI)

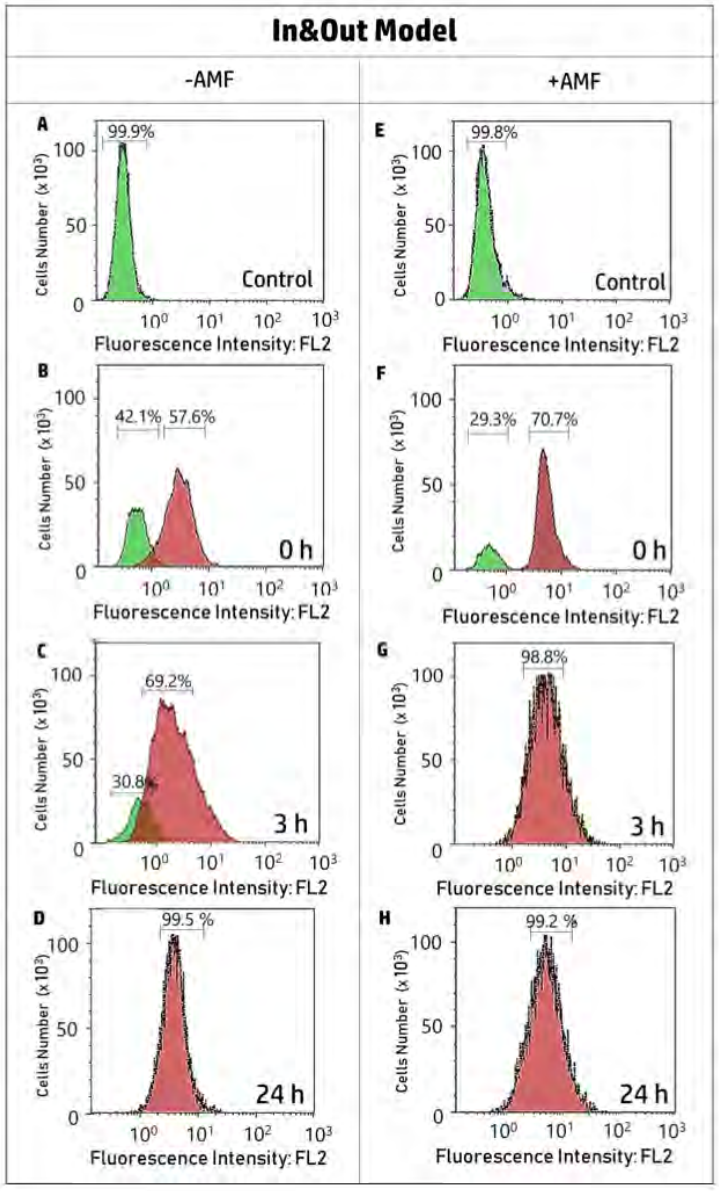

Fig. 4. Flow cytometry analysis of the time dependent nanoparticles uptake in the In&Out Model. Left: Cells without exposure to the AMF (-AMF), Right: Cells after the AMF exposure(+AMF). (A, E) Control cells without MNP, (B, F) 0 hours, (C, G) 3 hours, (D, H) 24 hours. Data have been selected as a representation of a series of five experiments.

220x365mm (72 x 72 DPI)

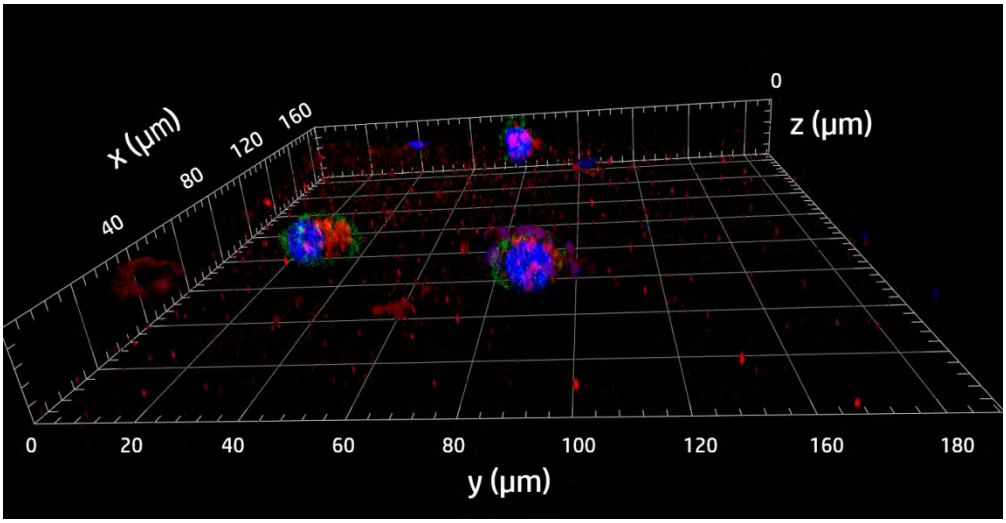

Fig. 5. 3D reconstruction of confocal images acquired for the In&Out Model 24 h after AMF exposure. The nucleus is shown in blue (DAPI), actin in green (Phalloidin_AlexaFluor488) and MNPs in red (TAMRA). The presence of MNPs is still observed outside the cells 24 h after the AMF exposure.

262x135mm (150 x 150 DPI)

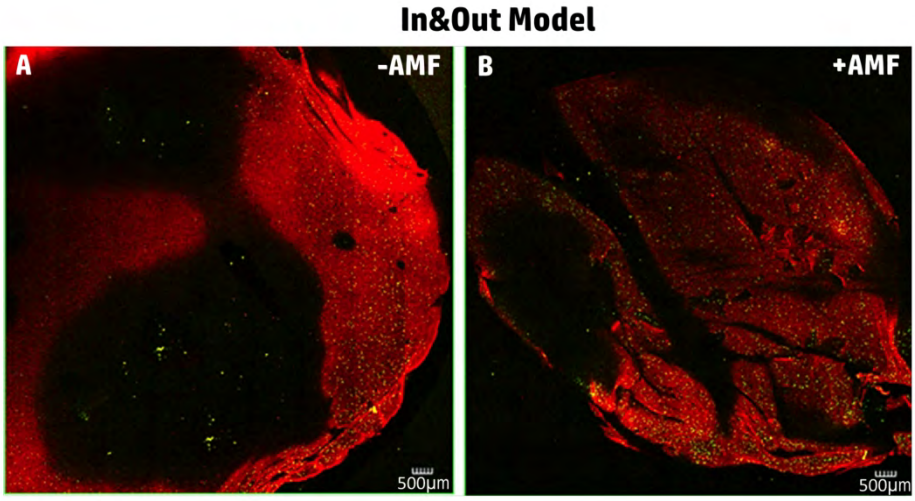

Fig. 6. Map image of confocal microscopy of 3D cell culture without (A) and with (B) the AMF exposure for the In&Out Model (0 hours). The image shows the overlay of two channels: green fluorescence of the labeled cells and red fluorescence of the MNPs. Scale bar is 500 µm.

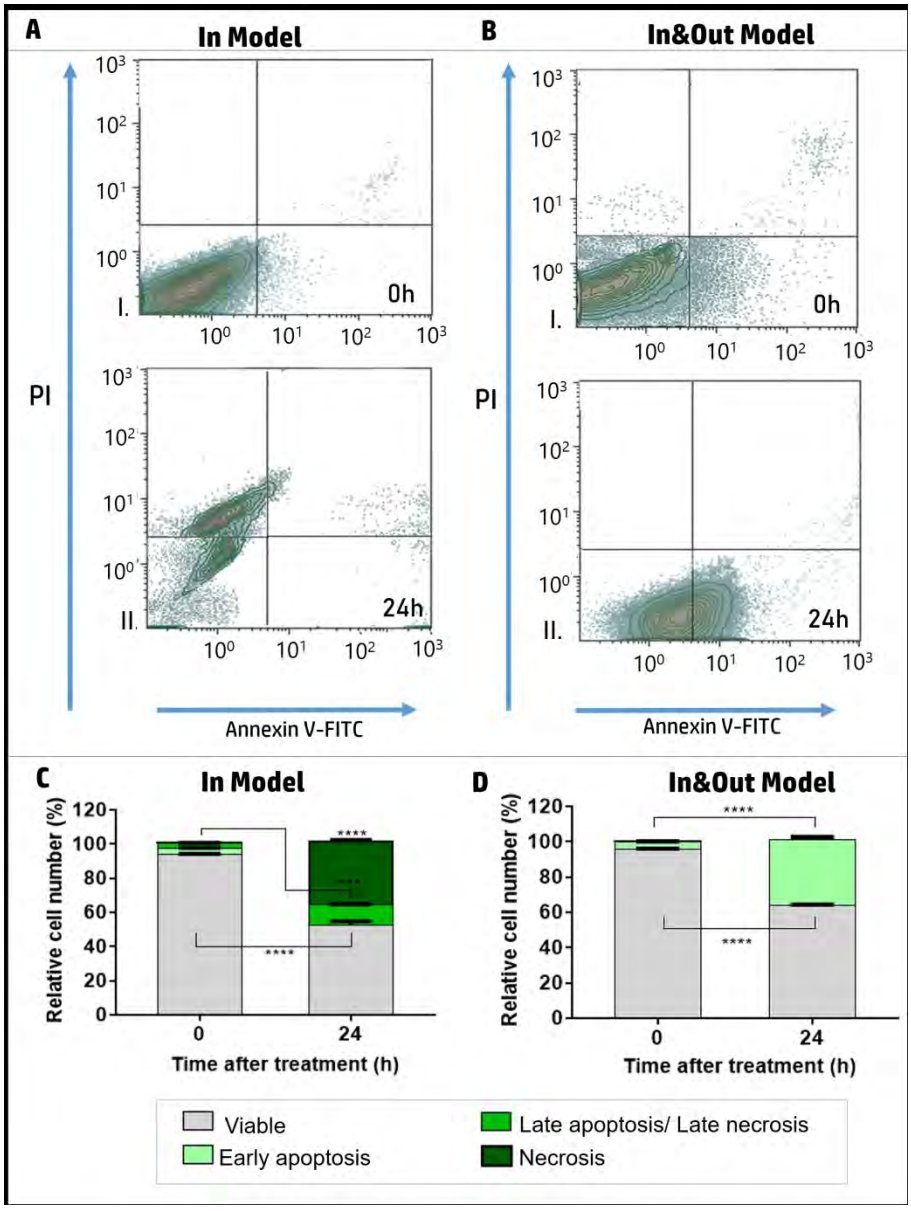

Fig. 7. Analysis of magnetic hyperthermia-induced cell death (Annexin V and PI staining). Selected density plot (representative of 5 experiments) obtained at 0h and 24h after MH treatment for the In Model (A) and In&Out Model (B). (C and D) Summarized flow cytometry data resulting from five independent experiments shown as mean ± SD. Statistical significance between the means at the different times was determined using a two-way ANOVA with Sidak's multiple comparisons test (**** $p < 0.0001$; *** $p < 0.001$; $p > 0.05$ no significance).

401x533mm (150 x 150 DPI)

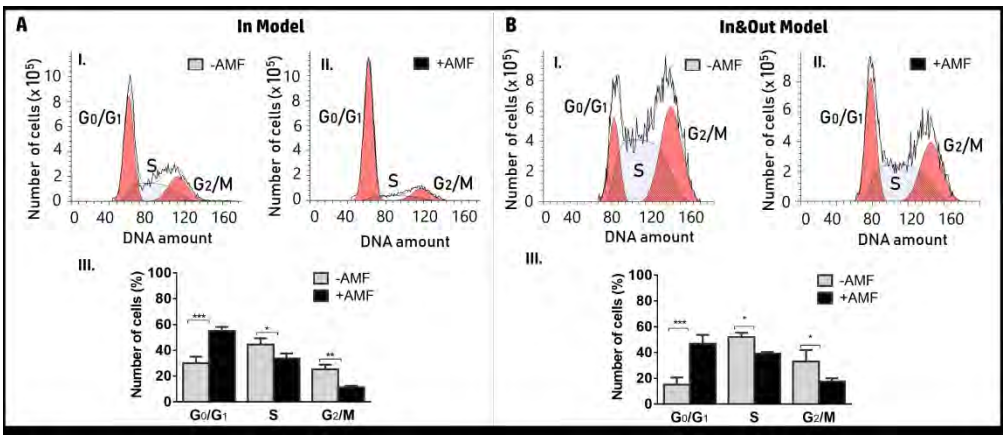

Fig. 8. Effect on cell cycle distribution 24 h after magnetic hyperthermia treatment. (A) In Model (B) In&Out Model. The distribution of cells in each phase is given in the case of no MH treatment (I); after MH treatment (II) and the comparison of both experiments (III). Results are represented as average ± S.D. and are based on three independent experiments. Statistical significance was determined using a one-way ANOVA with Bonferroni post-test (***p<0.001; **p<0.01; *p<0.05).

608x261mm (150 x 150 DPI)

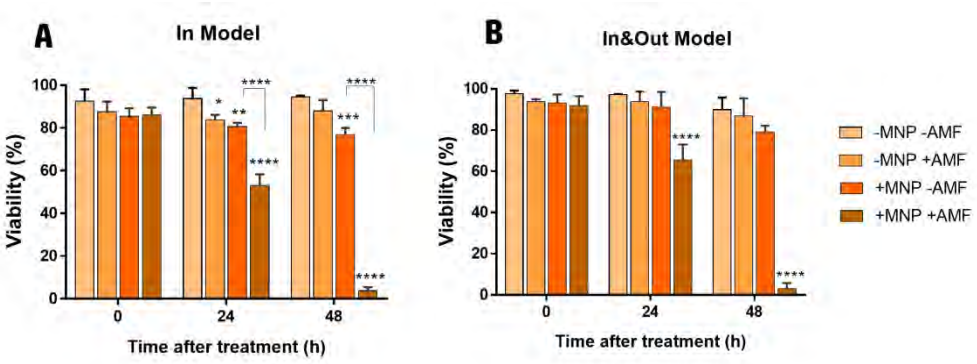

Fig. 9. MNPs cell viability evaluated in 3D models at different times after the Magnetic Hyperthermia treatment. (A) In Model and (B) In&Out Model. Cell viability has been evaluated by Flow Cytometry for the two models and compared different controls: with (+MNPs) or without (-MNPs) magnetic nanoparticles, and with (+AMF) or without (-AMF) exposure to the magnetic field. Results from five independent experiments are shown as mean ± SD. Statistical significance between the means respect to the control (-MNP -AMF) was determined using a two-way ANOVA with Dunnett's multiple comparisons test (****p<0.0001; ***p<0.001; **p<0.01; *p≤0.05; p>0.05 no significance). In cases where more than one group generated significant differences with respect to control, the means between those groups were also compared.

367x136mm (150 x 150 DPI)

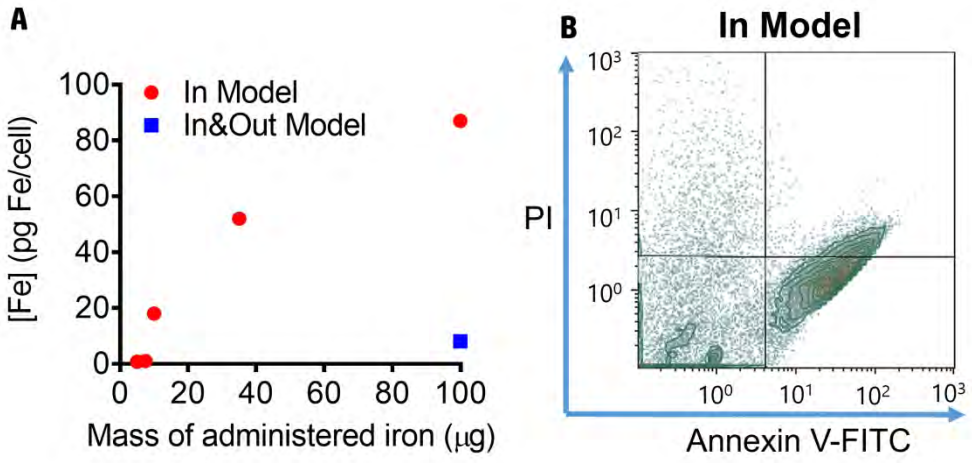

Fig. 10. Effect of the iron concentration inside the cells. (A) Intracellular iron content for both 3D models as a function of the administered iron amount. (B) Flow cytometry analysis of the cells in the In Model-lowFe (incubated with 10 times less MNPs) 24 h after MH treatment.

397x193mm (150 x 150 DPI)

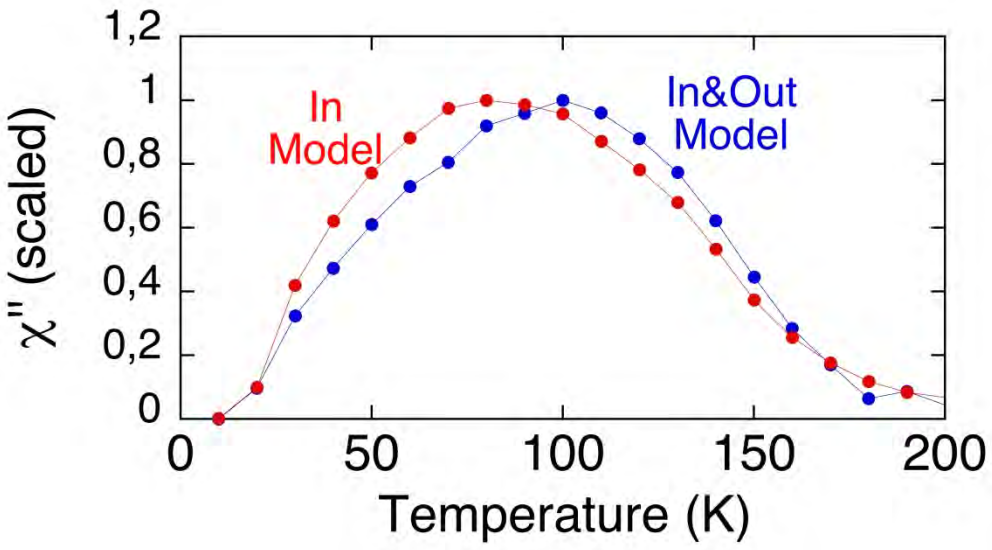

Fig. 11. Magnetic characterization of the 3D cell cultures. Temperature dependence of the out-of-phase susceptibility scaled to their maximum of the two different models.

332x184mm (288 x 288 DPI)